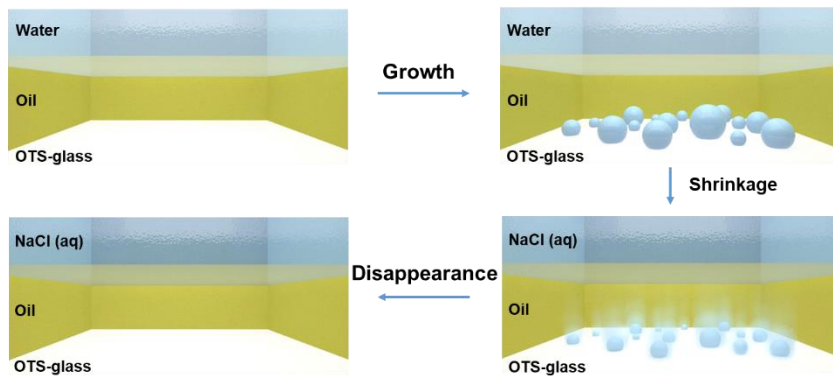


## Graphical Abstract



## The growth and shrinkage of water droplets at the oil-solid interface

Ran Zhang<sup>a</sup>, Wei Liao<sup>a</sup>, Yunpeng Wang<sup>a</sup>, Yao Wang<sup>a</sup>, D. Ian Wilson<sup>b\*</sup>, Stuart M. Clarke<sup>c\*</sup>, Zhongqiang Yang<sup>a\*</sup>

<sup>a</sup> Key Laboratory of Organic Optoelectronics and Molecular Engineering of the Ministry of Education, Department of Chemistry, Tsinghua University, Beijing 100084, China

<sup>b</sup> Department of Chemical Engineering and Biotechnology, Philippa Fawcett Drive, University of Cambridge, Cambridge CB3 0AS, UK

<sup>c</sup> Department of Chemistry and BP Institute, Madingley Rise, University of Cambridge, Cambridge, CB2 1EW, UK

\*Address correspondence to:

Stuart M. Clarke, [stuart@bpi.cam.ac.uk](mailto:stuart@bpi.cam.ac.uk)

D. Ian Wilson, [diw11@cam.ac.uk](mailto:diw11@cam.ac.uk)

Zhongqiang Yang, [zyang@tsinghua.edu.cn](mailto:zyang@tsinghua.edu.cn)

ABSTRACT

*Hypothesis*

The mechanism for the spontaneous formation of water droplets at oil/solid interfaces immersed in water is currently unclear. We hypothesize that growth and shrinkage of droplets are kinetically controlled by diffusion of water through the oil, driven by differences in chemical potential between the solid substrate and the aqueous reservoir.

*Experiments*

The formation, growth and shrinkage of water droplets at an immersed oil/solid interface are investigated theoretically and experimentally with three silicone oils. The surface is hydrophobic and the droplets formed are truncated spheres with radius,  $a$ , less than 10  $\mu\text{m}$ . The expansion and contraction of the droplets can be controlled by adjusting the difference in chemical potential. The growth kinetics are modelled in terms of water migration through the oil layer which predicts  $a^2 \propto t$ .

*Findings*

This is the first study of possible mechanisms for the formation of such interfacial droplets. Several possible causes are shown to be unfavourable, negligible or are eliminated by careful experiments controlling key parameters (such as oil viscosity, substrate chemistry). The rate constant for mass transport is proportional to difference in chemical potential and an estimate shows dissociation of surface groups on the substrate provides a driving chemical potential of the right magnitude.

Keywords: Interfacial droplets, Droplet growth, Droplet shrinkage, Oil-solid interface, Viscosity, Osmotic pressure, Chemical potential, Surface speciation, Diffusion

## 1. Introduction

When water is brought into contact with a hydrophobic surface in air, it will tend not to wet the surface and will form droplets with a contact angle greater than  $90^\circ$  [1–3]. When a hydrophobic surface is coated with a thin layer of a sparingly water-soluble oil and water added on top, a water/oil/solid sandwich structure is formed as shown in Fig. 1a. It is easy to accept that these three phases are immiscible and well separated or involves very little diffusion, however water droplets have been observed to form spontaneously over a period of hours to days at the oil/solid interface [4,5]. Yang *et al.* used confocal microscopy to track the growth of droplets with diameters typically between microns to tens of microns on a number of hydrophobic surfaces (contact angle greater than  $90^\circ$ ) [6]. The droplets increased in size by steady growth, although there was coalescence (accompanied by a decrease in number) when the droplets grew and touched each other.

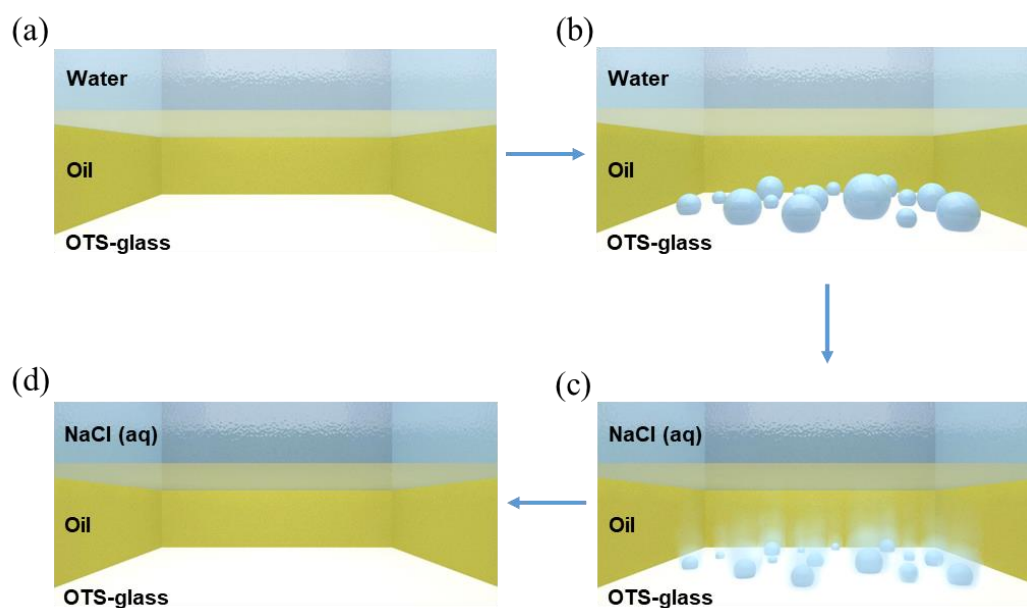


**Fig. 1** Schematic illustrations of (a) the initial condition, with a layer of oil between the lower solid substrate and upper water layer which leads to formation of water droplets at the oil/solid interface, shown in (b). On changing the water to NaCl solution the droplets shrink (c) and disappear (d).

The observance and the rate of droplet formation on related boundaries, such as liquid-vapour interfaces [7–9] and liquid-impregnated surfaces (LIS) [10–16], have

been investigated, but the reason why droplets would spontaneously form on oil-coated hydrophobic surfaces submerged in water is still unclear.

Here we present theoretical considerations and experimental evidence indicating that the formation and shrinkage of interfacial droplets on hydrophobic surfaces in such configurations is kinetically controlled by water migration through the oil phase. It is noted that glass was treated with octadecyltrichlorosilane (OTS) to obtain hydrophobic surfaces and silicone oils (polydimethylsiloxane) were chosen as the oil layer. This is not specific to OTS/silicone oil which is taken here as a convenient system to characterize the kinetics. Analysis of droplet shrinkage kinetics for a series of silicone oils indicates that growth and shrinkage of the drops can be controlled by adjusting the chemical potential of the aqueous reservoir. Interestingly, the chemical potential needed to drive shrinkage is demonstrated to be small – implying that a similarly small chemical potential is required to drive the process.

In addition, by comparing the behaviour on a number of well-characterised, related systems [17–23], we propose that the driving force for droplet formation is dissolution of species at the solid substrate surface into the water. This can include counter ion dissolution, and/or hydrolysis/surface speciation of surface chemical functionality (typically weak acids). We demonstrate that this mechanism is consistent with the small chemical potential difference needed to drive growth/shrinkage and leads to an effective maximum droplet size, as observed experimentally. This experimental and theoretical study on the formation and shrinkage of interfacial droplet kinetics could deepen our understanding of the multiple phase system, such as the original driving forces to create interfacial droplets, the kinetic models of mass transportation across interfaces [24,25]. Those findings would direct scientists to make surface supported colloids or micro-reactors [26,27] without using surfactants or mechanical input as conventional methods do. By controlling the formation and shrinkage of interfacial droplets, it provides a new approach to manipulate the diffusion of water molecules potentially for the application in oil-water separation [28,29], antifouling coating [30,31] etc.

## 2. Thermodynamic considerations

Anand *et al.* provide a useful summary of the free energy changes associated with droplet formation at interfaces, outlining why a water droplet would prefer to form at an oil/substrate interface rather than in the bulk oil unless the substrate is completely non-wetting [16]. The analysis is extended here to the water/oil/substrate reservoir ‘sandwich’ outlined above. On contact between the two liquids, water and oil will diffuse across the interface into the other phase. The sparing solubility of the components and relatively small volume of the oil layer will mean that the latter reaches saturation much earlier, and the water layer will still be effectively pure, as shown in Fig. 2a. When a water droplet nucleates on the surface it will give rise to a neighbouring region of oil which is depleted of water: water will diffuse towards this region and if the difference in chemical potential is favourable, it will be added to the droplet.

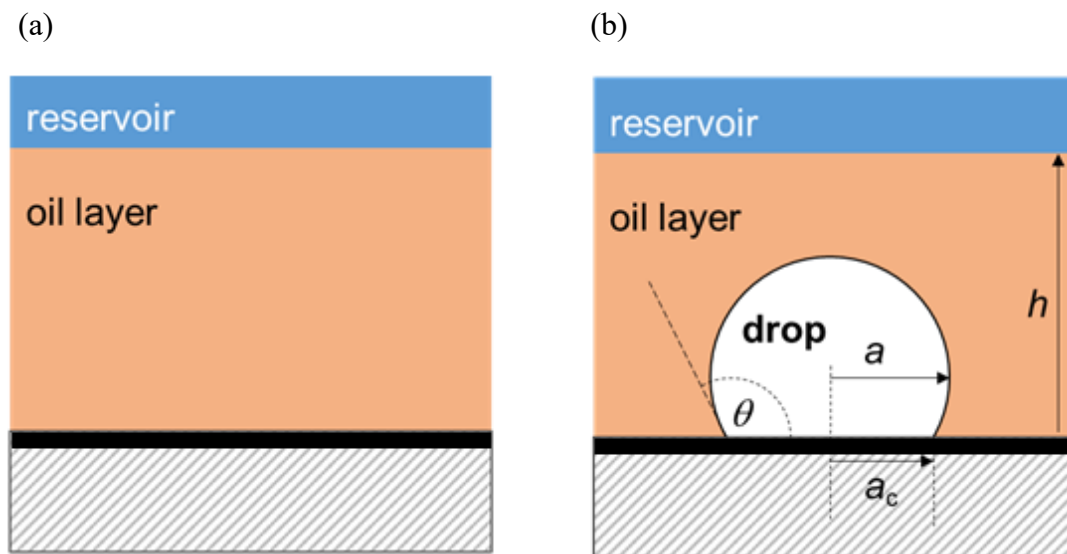


**Fig. 2.** Schematic of droplet formation. (a) Initially, the oil layer is in contact with pure water. Some of the water dissolves into the oil which can migrate to the liquid/solid interface and form a droplet. (b) Formation of water droplet with radius  $a$ , contact angle  $\theta$  and radius of contact line  $a_c$ . We anticipate that there will be a gradient in water concentration within the oil layer. The black region at the top of the substrate indicates the hydrophobic OTS layer.

Consider the idealized case shown in Fig. 2b, where a droplet (a truncated sphere) of radius  $a$  and volume  $V_d$  is formed from a region of initially water-saturated oil. The system is isothermal. In the absence of contact line pinning, droplets in the sandwich

will be spherical as the capillary length scale is of order mm<sup>1</sup>. The *overall* change in free energy on forming a droplet on the surface is given by

$$\Delta G = n_{w,d}\mu_{w,d} + n_{o,d}\mu_{o,d} - n_{w,d}\mu_{w,b} - n_{o,d}\mu_{o,b} + \Delta E \quad [1]$$

where  $n_{i,j}$  refers to the number of moles and  $\mu_{i,j}$  the chemical potential of component  $i$  in phase  $j$ :  $\Delta E$  is the surface energy associated with the formation of the water-oil and water-substrate interfaces. Subscript  $d$  refers to the droplet and  $b$  to a bulk phase;  $o$  refers to oil and  $w$  to water. This expression considers the driving force for water to be transferred from the bulk layer into the droplet: the variation in chemical potential of water (and oil) across the layer is not considered and suffices for this purpose.

For a spherical droplet with radius  $a$  and contact angle  $\theta$ , the volume of the droplet is (see Anand *et al.*, 2015)

$$V_d = \frac{\pi a^3}{3} (2 + \cos\theta)(1 - \cos\theta)^2 = \frac{\pi a^3}{3} \psi \quad [2]$$

and  $\Delta E$  is given by

$$\Delta E = 2\pi a^2 (1 - \cos\theta) E_{ow} - \pi a^2 \sin^2\theta (E_{os} - E_{ws}) \quad [3]$$

where  $E_{ow}$ ,  $E_{os}$  and  $E_{ws}$  are the surface energies of the oil-water, oil-substrate and water-substrate interfaces, respectively and  $\psi$  is a shape factor associated with the geometry of the drops. Substituting for the latter terms using Young's equation [32],  $E_{os} = E_{ws} + E_{ow}\cos\theta$ , yields  $\Delta E = \pi a^2 \psi E_{ow}$ . Note that this energy change is always positive, *i.e.* is unfavourable.

Here we refer to substrates as hydrophobic when the contact angle is greater than 90°, and hydrophilic when the contact angle is less than 90°. The assumption of spherical droplets on hydrophobic surfaces is supported by the observations of Li *et al.* [33], who measured contact angles of water droplets on a range of surfaces in bulk *n*-hexadecane and in water/*n*-hexadecane sandwiches: those formed on hydrophobic surfaces were spherical. The values on hydrophilic surfaces, however, differed owing to contact line

---

<sup>1</sup> The capillary length,  $l_c$ , is the length scale at which hydrostatic pressure is equal to capillary pressure:  $l_c = \sqrt{\sigma/g\Delta\rho}$ , where  $\sigma$  is the interfacial tension and  $\Delta\rho$  is the difference in liquid densities. For the silicone oils and water employed in this work,  $\sigma \sim 40 \text{ mN m}^{-1}$  [44],  $\Delta\rho \sim 29\text{-}82 \text{ kg m}^{-3}$  and  $l_c \sim 7.3\text{-}12.5 \text{ mm}$ .

pinning.

The volume of the droplet is given by

$$V_d = n_{w,d}\bar{V}_{w,d} + n_{o,d}\bar{V}_{o,d} \quad [4]$$

where  $\bar{V}_{ij}$  is the partial molar volume of species  $i$  in phase  $j$ . The oil is sparingly soluble in water: for  $n$ -hexadecane in water at 25 °C and 1 bar, the mol fraction of water in  $n$ -hexadecane at saturation is  $9.4 \times 10^{-4}$  [34] while that of  $n$ -hexadecane in water is of the order  $10^{-10}$  [35]. Silicone oils are similarly sparingly soluble in water [36] but the water content of silicone oils can be several hundred ppm (Gelest, Inc., [37]). Hence  $n_{o,d} \ll n_{w,d}$  giving

$$V_d \approx n_{w,d}\bar{V}_w \quad [5]$$

and

$$n_{w,d} \approx \frac{\pi\psi}{3\bar{V}_w} a^3 \quad [6]$$

The contribution from the chemical potential of the oil in Equation [1] is therefore expected to be small. Combining the above results yields

$$\Delta G = \frac{\pi\psi}{3\bar{V}_w} a^3 \left\{ (\mu_{w,d} - \mu_{w,b}) + \frac{3\bar{V}_w E_{ow}}{a} \right\} \quad [7]$$

The difference in water chemical potential is given by

$$\mu_{w,d} - \mu_{w,b} = RT \ln \frac{\gamma_{w,d} x_{w,d}}{\gamma_{w,b} x_{w,b}} + \bar{V}_{w,d} (2\sigma_{ow}/a) \quad [8]$$

where  $R$  is the gas constant,  $T$  is the absolute temperature,  $\gamma_{w,i}$  is the activity coefficient for water in phase  $i$ , and  $x_{w,j}$  is the mol fraction of water in phase  $j$ . The second term on the RHS is the contribution to the chemical potential from the Laplace pressure in the drop, where  $\sigma_{ow}$  is the oil-water surface tension<sup>2</sup>. For simple interfaces such as those present here,  $\sigma_{ow} = E_{ow}$ . Since the water is almost pure in both phases,  $\gamma_{w,d} \approx 1$ . Assuming the bulk water to be pure and there to be only two species (oil and water)

---

<sup>2</sup>The contribution can be calculated from  $\left(\frac{\partial \mu}{\partial P}\right)_T = \bar{V}$ : assuming that  $\bar{V} = \bar{V}_{w,d}$ , one obtains  $\mu = \mu^0 + \bar{V}_{w,d}(P - P^0) = \mu^0 + \bar{V}_{w,d}(2\sigma_{ow}/a)$ .



present in the droplet, one can write  $\ln x_{w,d} = \ln(1 - x_{o,d}) \approx -x_{o,d}$  and thus

$$\Delta G = \frac{\pi\psi}{3\bar{V}_w} a^3 \left\{ \frac{5\bar{V}_w E_{ow}}{a} - RT x_{o,d} \right\} \quad [9]$$

Inspection of Equation [9] provides key insight into a possible mechanism (assuming no other contributions to  $\Delta G$  arise). The droplets cannot contain pure water ( $x_{o,d} = 0$ ), as the RHS (right hand side) would then be positive, indicating that droplets should *not* form spontaneously. For a sparingly soluble oil, the minimum droplet nucleation size required for growth,  $a^*$  can be calculated by setting  $\Delta G = 0$ . For droplets smaller than  $a^*$ , the first (positive) term will dominate and promote re-dissolution. Only droplets bigger than  $a^*$  will be expected to survive. For *n*-hexadecane in water at 25 °C, taking the mole fraction of *n*-hexadecane in water at saturation as  $10^{-10}$  and  $E_{ow}$  as 53.5 mN/m [38], this gives

$$a^* \approx \frac{5\bar{V}_w E_{ow}}{RT} \frac{1}{x_{o,d}} \quad [10]$$

$$a^* \approx \frac{5 \times 1.8 \times 10^{-5} \times 0.05}{8.314 \times 298} \frac{1}{1 \times 10^{-10}} \sim 19 \text{ m}$$

A similar calculation for a silicone oil with molecular mass 6000 and mole fraction of silicone oil in water at saturation is  $2 \times 10^{-11}$  [36] would give  $a^* \sim 90$  m. Hence, we conclude that the minimum droplet size required for growth is very large indeed, and it is clear that there must be a further contribution to  $\Delta G$  to make droplet formation favourable.

Buoyancy contributions to droplet formation can be neglected by a simple comparison of the surface energy associated with a droplet and the potential energy gained by the same volume of water descending the distance of the film thickness,  $h$ , under gravity,  $\Delta PE$ . Considering a droplet of radius 1  $\mu\text{m}$  in an oil film of thickness 30  $\mu\text{m}$ , such as observed in this work, gives

$$\frac{\Delta E}{\Delta PE} = \frac{\pi a^2 E_{ow} \psi}{\frac{1}{3} \pi a^3 \psi g h \Delta \rho} = \frac{3 E_{ow}}{a g h \Delta \rho} = \frac{3 \times 0.04}{1.0 \times 10^{-6} \times 9.8 \times 30 \times 10^{-6} \times 230} \approx 2 \times 10^6 \quad [11]$$

The negligible effect of gravity is confirmed by the experimental observation that droplets are formed if the oil-coated surface is above the water (data not shown).

Two methods were explored to determine the chemical potential associated with the droplet phase. The first was to add a solute to the water in the reservoir, thereby reducing the water's chemical potential, to determine what concentration inhibited the appearance of droplets. This approach to determine the chemical potential (or osmotic pressure) of the droplet phase is time consuming and also includes a contribution associated with overcoming the nucleation barrier.

The second method was to track the shrinkage of droplets initially formed on hydrophobic OTS layers in a sandwich of water-silicone oil-OTS substrate, following the substitution of the water reservoir by an aqueous solution of NaCl. A diffusion model (see Supplementary data) has been developed and gives the relationship

$$\frac{da}{dt} = \frac{2KD}{\psi a} \frac{\bar{V}_w}{\bar{V}_o} \frac{\bar{V}_w \Delta \Pi}{RT} = \frac{k_2}{a} \Delta \Pi \quad [12]$$

where  $\Delta \Pi$  is the difference in osmotic pressures between the reservoir and the droplet phases,  $K$  is equilibrium constant and  $D$  the diffusivity of water in oil. A plot of  $a^2$  against time  $t$  should be linear with gradient proportional to  $\Delta \Pi$ . The derivation is similar to that of the model of Miyazaki and Inasawa [39], for shrinkage of droplets in a thin oil layer. Its application to water droplets shrinking by diffusion through layers of silicone oil was demonstrated by Harz and Knoche [40]. Conducting tests with different salt concentrations allows the osmotic pressure associated with zero growth to be determined, eliminating the contribution from nucleation, and hence allows the osmotic pressure driving droplet formation to be identified.

### 3. Materials and methods

#### 3.1. Materials

Square glass microscope coverslips (22 mm × 22 mm, Cat., #72204-1) and gold grids (20 μm thickness, 333 μm pitch, and 55 μm bar width) were obtained from Electron Microscopy Sciences (Hatfield, PA, USA). Silicone oils with molecular weights 770, 6000 and 28000 were purchased from Alfa Aesar (Ward Hill, MA, USA). OTS and calcein AM were purchased from Sigma Aldrich (Milwaukee, WI, USA). Heptane (HPLC grade) was purchased from Fisher Scientific (Pittsburgh, PA, USA). Other

chemicals were obtained from local companies with AR grade or above. Milli-Q water (18.2 M $\Omega$ ·cm) was used. Physical properties of silicone oils are summarized in Table 1.

**Table 1** Physical properties of test oils, at 25 °C unless otherwise indicated.

Oil	Silicone oil		
	Molecular weight	770	6000
Saturated water content (ppm) [41]	2558	560	170
Density (kg·m <sup>-3</sup> )	918	950	971
Dynamic viscosity (mPa·s)	4.6	95	970
Contact angle on OTS-glass in air (°)	11.2 ± 0.2	14.0 ± 0.6	15.3 ± 0.7
Surface tension in air (mN/m) [42]	21.1	21.3	21.4
Surface tension in water (mN/m) [43,44]	41.5	41.4	40.0
Capillary length in air (mm)	7.3	9.5	12.5

\*Density and dynamic viscosity are from Alfa Aesar website.

### 3.2. Modification of substrates

The microscope cover glass was immersed in piranha solution (a 7:3 v/v mixture of H<sub>2</sub>SO<sub>4</sub> and H<sub>2</sub>O<sub>2</sub>) and heated to 80 °C for an hour, then dried at 100 °C oven for an hour, resulting in piranha cleaned glass. The glass was characterised before and after immersion in piranha solution by AFM (Bruker, MultiMode 8, RTESP, tapping mode in air), see Fig. S1. The piranha cleaned glass was immersed in a 5 mM solution of OTS in heptane at ambient condition around 25 °C for 30 min, rinsed with heptane, then dried in air at 100 °C in an oven. OTS-glass was obtained. The roughness of the coated substrates was measured by AFM and gave a root mean square roughness (RMS) of 8.30 nm over an area of 10 × 10 μm<sup>2</sup>, (topography image in Fig. S2) which was consistent with previously reported values [6]. No detectable effect was found for the influence of roughness on the formation of interfacial droplets.

Here we also discuss results from a number of self-assembled monolayers (SAMs) on gold substrates, reported previously [45]. These include a bare gold substrate and the same gold substrate reacted with a number of alkyl thiols, with particular

functionality on the other end of the molecule to the thiol group. The approach here results in grafted molecular layers with the thiol group attaching to the gold and the other end presenting a particular functionality to the adjacent fluid. These functionalities are (a) straight alkyl chain, (b) quaternary ammonium halide, (c) fatty acid and (d) primary alcohol.

### 3.3. Contact angle measurement

Static contact angles of water and oils on OTS-glass were measured using 3  $\mu\text{L}$  droplets at room temperature using a goniometer (OCA 15 plus, software SCA20, Dataphysics Instruments). The contact angles of water and silicone oil ( $M = 770, 6000, 28000$ ) on OTS-glass in air were measured as  $110.0 \pm 0.2^\circ$ ,  $11.2 \pm 0.2^\circ$ ,  $14.0 \pm 0.6^\circ$ ,  $15.3^\circ \pm 0.7^\circ$ , respectively, confirming that the OTS surface was hydrophobic and oleophilic (see Supplementary Table S1). The contact angles reported here were the average of at least three measurements. Droplets formed on OTS-coated glass immersed in oil were imaged *in situ* using an inverted laser scanning confocal microscope (LSCM) and their contact angles were calculated from the three dimensional (3D) images by ImageJ software. Measurements were made with a reservoir solution of 1 M NaCl as a compromise between competing effects: (i) higher concentrations, which caused fast shrinkage, but made it difficult to scan the droplets accurately as they shrank, and (ii) lower concentrations, which gave slower shrinkage but imaging was subject to quenching of the fluorescence.

### 3.4. Formation of interfacial droplets

The protocol was based on that reported by Yang *et al.* [6]. Culture dishes were prepared with a 10 mm diameter hole cut out of the centre of the base and the OTS-glass test piece was glued in place across this hole (see Supplementary Fig. S3). The gold grid was placed on the OTS surface and silicone oil added dropwise to the grid. Any excess was removed by a syringe in order to give a uniformly filled grid. 4 mL of milli-Q water was then added to the culture dish to immerse the test piece and grids and generate the sandwich. The sample was incubated in an environmental chamber

(temperature: 25 °C, relative humidity: 50%). The thickness of the oil layer was measured by confocal microscopy (see below). The thicknesses ranged from 18 to 79  $\mu\text{m}$  (see Table S2). Thicker layers could be used but resulted in slow droplet growth. After several days' incubation droplets grew to between 10 and 20  $\mu\text{m}$  in diameter. These largest drops are a significant fraction of the oil layer thickness and hence we may expect some deviation from growth kinetics based on the model proposed here. However, the early time growth is still expected to be in accordance with the model.

### *3.5. Optical and confocal imaging of interfacial droplets*

A Nikon ECLIPSE Ti microscope with a digital camera (Nikon DS-U3) and a differential interference contrast prism were used to monitor the appearance, growth and shrinkage of droplets on the OTS surface. In order to obtain 3D profiles of interfacial droplets, a fluorescent dye, calcein AM, was added to the aqueous reservoir to give a calcein AM concentration of 2  $\mu\text{M}$ . The dye diffused into the droplets, enabling visualization with a Zeiss LSM800 with Airyscan model LSCM (em: 515 nm, ex: 488 nm). The two dimensional (2D) and 3D confocal images were analysed using Zen blue software. The thickness of the oil layer could also be determined from the 3D confocal fluorescent images. The variations in droplet behaviour with the dye exhibited no more variation than variations in the droplet growth without the dye. However, there was some evidence that migration of the dye through the oil to the droplets was slower than the water, which prevents very short time droplet growth to be addressed using the confocal method employed here.

### *3.6. Shrinkage and disappearance of interfacial droplets*

Droplets were grown for 10 days, after which the reservoir water was replaced by NaCl solutions with concentrations of 0.50 M, 0.75 M, 1.00 M, 1.50 M and 2.00 M. This arrangement caused the droplets to shrink and ultimately disappear. Images of the shrinking droplets were taken every minute. A Matlab program was used to identify each droplet in the optical micrographs and extract its diameter. Since the contact angle

was normally greater than  $90^\circ$ , this gave the droplet radius as a function of time,  $a(t)$ . The code is provided in the supplementary materials. Four droplets with initial diameters greater than  $10\ \mu\text{m}$  were selected from each test for comparison with the model.

## 4. Results and discussion

### 4.1. Inhibition of droplet formation

We study the droplet growth kinetics in order to gain insight into the process. As noted previously, nucleation and growth of water droplets both occur at the oil/substrate interface. However, the kinetics of nucleation are relatively complex and are stochastic in nature. Hence, we consider droplet shrinkage where there are no nucleation issues. Addition of salt to the water reservoir essentially pulls water from the droplets and this approach can be used to confirm and quantify the chemical potential driving force for droplet growth (and shrinkage). A number of solutes can be used: here we report results obtained with aqueous solutions of NaCl forming the aqueous reservoir. Migration of NaCl through the oil is possible but was not determined.

This approach can also be used to estimate the chemical potential driving force for droplet growth, by determining the reservoir conditions that inhibit the formation of droplets. This measure will include a contribution for nucleation so will be an overestimate. Droplet formation was inhibited at saline concentrations above  $250\ \text{mM}$  (osmotic pressure  $1\ \text{bar}$ ), see Fig. S4. This is much larger than the osmotic pressure obtained from shrinkage tests, indicating that the nucleation barrier is significant.

### 4.2. Droplet shape during shrinkage

The contact angle of the interfacial droplets undergoing shrinkage was studied with a reservoir NaCl concentration of  $1\ \text{M}$ . It was not possible to determine shape during the initial phase of droplet growth as the dye diffused less quickly than water. Droplets with initial radius of  $6.3$ ,  $5.8$  and  $6.0\ \mu\text{m}$  in silicone oils 770, 6000 and 28000, respectively, were monitored and gave the series of images presented in Fig. 3.

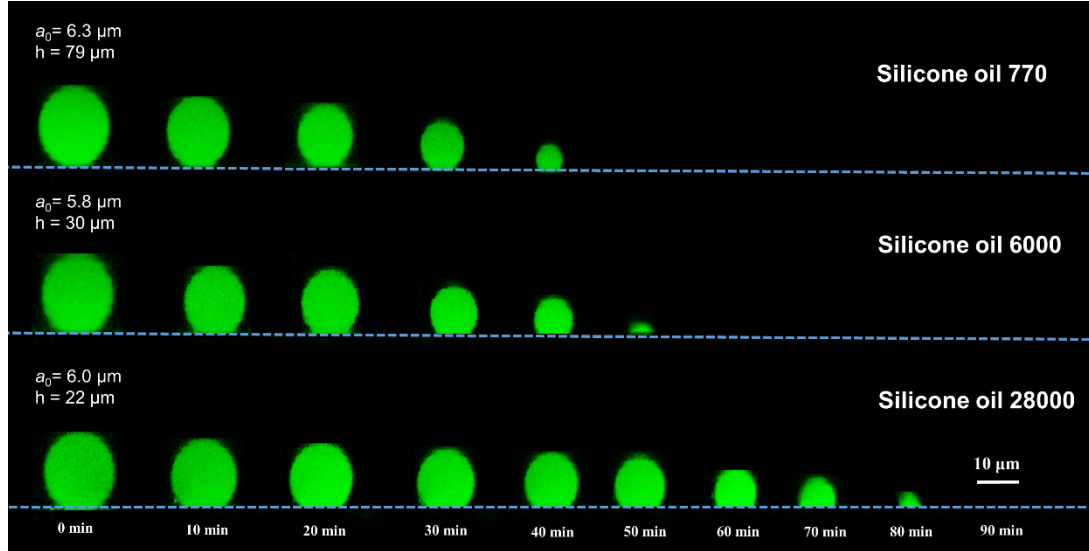


**Fig. 3.** Fluorescence images of shrinking interfacial droplets on OTS-glass with 1 M NaCl in the reservoir at the times indicated. ( $a_0$  refers to initial radius of droplets and  $h$  refers to the thickness of oil layer).

Whilst there is some modest image distortion due to the confocal optics, inspection of the droplet shapes confirmed that they were approximately spherical as they shrank. Initially the contraction occurs with a constant contact angle (CCA). In the later stages of shrinkage the contact angle was observed to decrease and the footprint of the droplet on the substrate remained constant (CCR). We examined sets of droplet growth data for similar behaviour but only CCA behaviour was observed. This may be because the very early growth kinetics are inaccessible due to the slow migration of the fluorescent dye used to label the droplet: the droplets may then become visible when larger than the range where CCA behaviour might be expected.

The evolution of the contact angle and the wetted radius (length  $a_c$  in Fig. 2b) of the shrinking droplets are plotted in Fig. 4 and show three stages:

- (i) CCA, where  $a_c$  decreases with time, with constant average contact angles of  $132.6 \pm 1.2^\circ$  ( $M = 770$ ),  $130.1 \pm 3.2^\circ$  ( $M = 6000$ ) and  $129.0 \pm 1.3^\circ$  ( $M = 28000$ ). The OTS surface remained non-wetting. This observation was consistent with previous reports which reported  $131 \pm 3^\circ$  [4];

- (ii) Constant contact radius (CCR), where the contact line is pinned and the contact angle decreases with time, with  $a_c = 3.2 \mu\text{m}$  ( $M = 770$ ),  $3.6 \mu\text{m}$  ( $M = 6000$ ) and  $2.9 \mu\text{m}$  ( $M = 28000$ );
- (iii) A final stage where shrinkage was too fast to image.

Transitions between CCA and CCR behaviour have been reported in studies of droplet evaporation on smooth hydrophobic surfaces [46–50]. Chen *et al.* reported the transition from CCR to CCA behaviour as their droplets shrank on surfaces structured at the micron scale, at length scales associated with the structures [47]. Their work differs from this study in that the opposite (CCA-CCR) transition was observed here and the surfaces are smooth, with no physical feature associated with a 5-7  $\mu\text{m}$  length scale.

The shrinkage model in the next section assumes CCA behaviour, with a constant relationship (the factor  $\psi$ ) between the interfacial area and droplet volume, which does not hold in the CCR stage. The shrinkage model was therefore not fitted to data in the CCR stage. The droplets disappeared after 50 min, 60 min and 90 min, respectively. The small effect of  $M$  on the shrinkage rate is discussed in the next section.



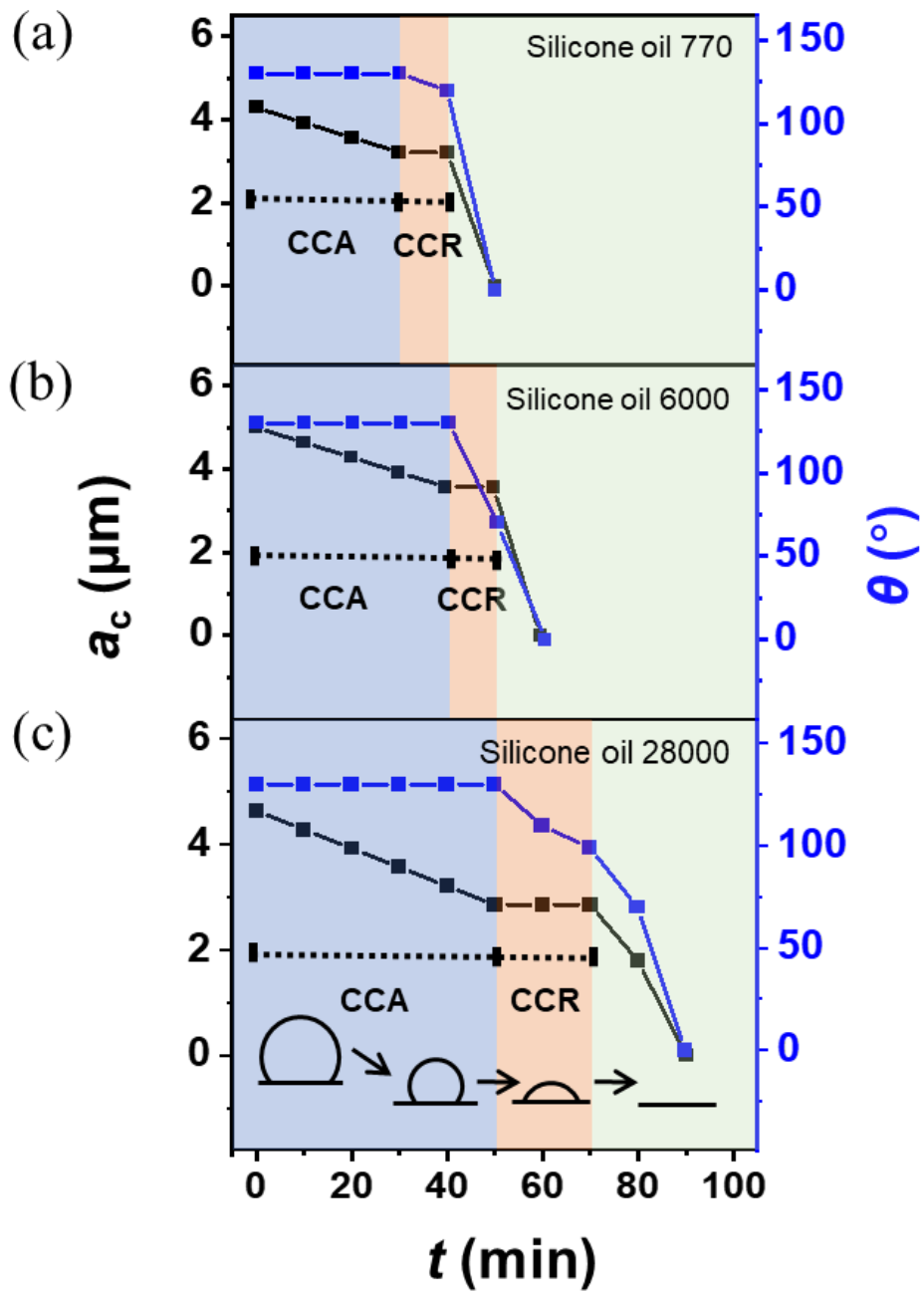


**Fig. 4.** Evolution of the contact radius,  $a_c$ , and contact angle,  $\theta$ , during shrinkage of droplets (corresponding to the interfacial droplets in Fig. 3) subject to 1 M NaCl in silicone oil layers with (a)  $M = 770$ , (b)  $M = 6000$ , and (c)  $M = 28000$  including schematic illustration of the different regimes.

### 4.3. Droplet growth and shrinkage

Fig. 5 shows examples of droplet growth in silicone oil ( $M = 6000$ ) plotted in the form suggested by the kinetic model given in the Appendix, [A10; A13]:

$$a^2 = a_0^2 + Bt \quad [12]$$

with  $a^2$  estimated from  $V^{2/3}$  (these early tests did not measure explicitly). The data show the initial linear trend expected for diffusion-controlled growth followed by an approach to a limiting size. Growth is slow, with gradients of order  $7 \times 10^{-12} \text{ m}^2\text{s}^{-1}$  in silicone oil. Droplet growth profiles for silicone oils with  $M = 770$  and  $28000$  are provided in Fig. S5 and Fig. S6, respectively.

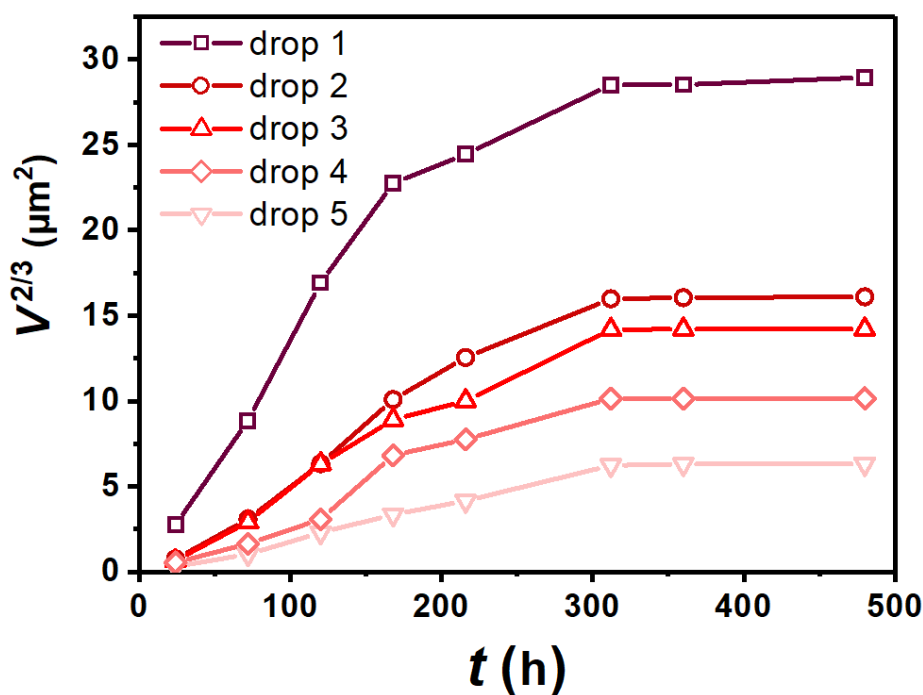


**Fig. 5.** Examples of droplet growth, time post nucleation, in silicone oil 6000.

Fig. 6a-c shows examples of droplets formed at silicone oil ( $M = 770, 6000, 28000$ ) – OTS-coated glass film interfaces shrinking in response to the reservoir being changed to a saline solution. Examples of images showing droplet appearance as they grow and shrink are available in Fig. S7 ~ Fig. S9. The data in this case are plotted in terms of the measured radius. We also present the  $a^2$  vs  $t$  trend, predicted by the model, and again find excellent agreement, Fig. 6d-f.

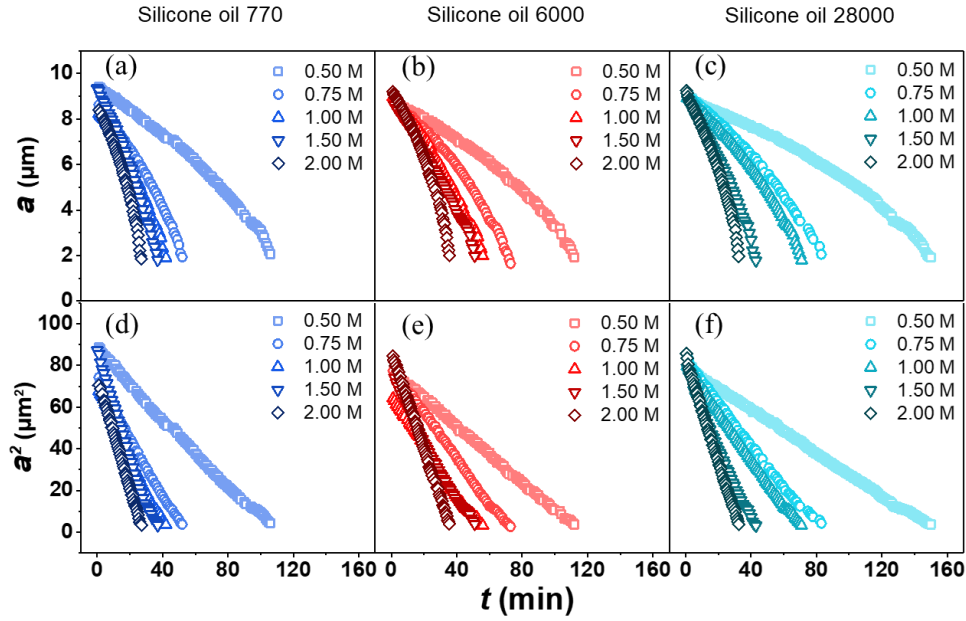


**Fig. 6.** Effect of reservoir NaCl concentration on evolution of droplet radius (a-c) and squared radius (d-f) for droplets formed in silicone oil layer with molecular weight of 770, 6000 and 28000, respectively.

The data for the CCA stage from the shrinkage of interfacial droplets under NaCl solution experiments were fitted to the model and the magnitude of the gradient,  $B$ , determined for each case. It was noticeable that large droplets (with  $a_0 > h/2$ ) gave large values of  $B$ , which is associated with short diffusion lengths so these were not considered further. The values are plotted against the osmotic pressure of the reservoir in Fig. 7 and show a strongly linear dependence on  $\Pi$ , which is consistent with Eqn. [A11]

There is noticeable scatter in the data, but all three silicone oils exhibit the linear relationship between  $B$  and  $\Delta\Pi$  predicted by the model. Interestingly, extrapolating the trends in each case to  $B = 0$  gives  $\Delta\Pi \sim 0$ , indicating that a very small chemical potential in the water reservoir is needed to cause the drops to shrink. This strongly suggests that the source of chemical potential driving droplet growth is small.

This experiment addressing the droplet shrinkage is convenient as it does not require consideration of nucleation kinetics that would have been important with droplet appearance and growth on the initially base oil/solid interface.

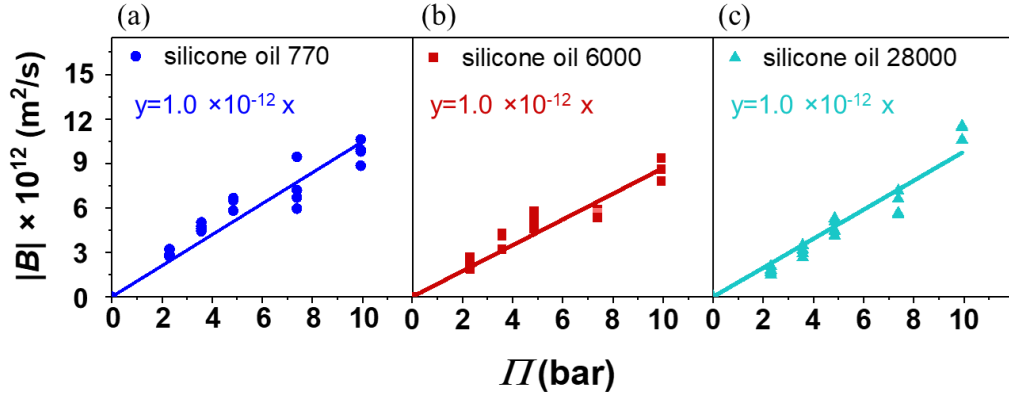


**Fig. 7.** Growth constant values obtained from shrinkage studies such as Fig. 6 with silicone oil molecular weight of (a) 770, (b) 6000 and (c) 28000.

Significantly, our data indicate that the gradients of the  $B$  and  $\Delta\Pi$  plots for the three silicone oils are similar, even though the three oils have very different viscosities. At first sight one might have expected that the diffusion of water through the silicone oil is governed by Stokes-Einstein behaviour and hence strongly dependent on the oil viscosity. The model derivation shows that Stokes-Einstein behaviour, as expressed in the Wilke-Chang result [51] yields  $B \propto M^{-2}\Delta\Pi$ , Equation [A13], which is not observed for the 38-fold difference in  $M$  here. There is, however, evidence from the literature that the mobility of water in silicone oils does not follow the Stokes-Einstein relation. Harz and Knoche studied shrinkage of water droplets in silicone oils with kinematic viscosities of 9.6 and 10350 cSt, corresponding to an  $M$  ratio of 105 [40]. They reported permeability coefficients – effectively the product of the Henry’s law constant and diffusion coefficient of  $45.8 (\pm 2.4)$  (9.6 cSt oil) and  $29.5 (\pm 1.6) \times 10^{-9} \text{ m}^2\text{s}^{-1}$ , *i.e.* a 35% decrease for a 105-fold increase in  $M$ . The permeability coefficients for silicone oils were 1-2 orders of magnitude larger than those obtained for mineral oils and are consistent with the literature on water vapour transport through siloxane liquids [52]. Hence we can explain the similarity in the experimentally determined gradients of the  $B$  and  $\Delta\Pi$  plots as arising from the similarity of the water mobility in these fluids.

#### 4.5. Discussion

We present in Fig. 8 the images of water droplet growth on a series of gold substrates

with/without SAMs used to confer well defined surface chemistry, previously reported by our group [45]. In all cases the water/oil and other aspects were as similar as possible. The Figure clearly indicates that the nature/chemistry of the substrate plays a key role in droplet formation.

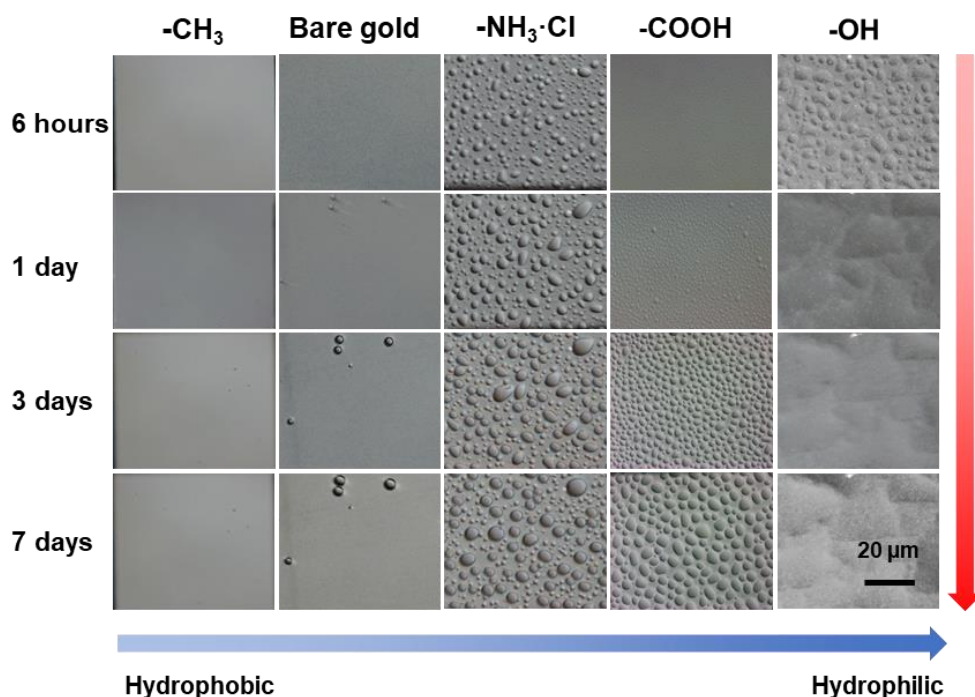


**Fig. 8.** Droplet formation on gold and gold with different SAMs. From left to right: alkyl chain, bare gold, quaternary ammonium halide, fatty acid, and primary alcohol. Droplet formation over time is shown in the figure. Reproduced from Ref. 45 with permission from the Royal Society of Chemistry.

Very few drops form on the bare gold and the alkylated surfaces, in contrast to the ammonium salt, where many drops are generated. Similarly, the fatty acid also forms many drops, but not as many as the ammonium salt. Droplets form rapidly on the primary alcohol and merge to form an (essentially wetting) water film.

This variation in droplet formation behaviour may be attributed to surface chemistry, particularly the release of ions from the surface into the droplet. In this work, the water is essentially pure and hence there is no background electrolyte. If this dissociation/dissolution of surface groups occurs, it will present a favourable chemical potential that may provide the driving force required. In the Supplementary data we calculate the extent of such dissolution and the resultant osmotic pressure. For a 1

micron droplet and  $90^\circ$  contact angle, the osmotic pressure is calculated to be approximately 0.1 bar. As discussed in section 4.3 and illustrated in Fig. 7, only a small chemical potential is required to drive droplet shrinkage, comparable with this calculation. Hence, we can expect that any significant competing chemical potential, e.g. from dissolved NaCl in the reservoir, will prevent droplet growth and lead to shrinkage, as observed in Fig. 7. We note that the initial nucleation of water drops from an initially dry surface will have an additional activation barrier and require a more significant chemical potential than that required to shrink the drops.

For the substrates in Fig. 8, we expect the bare gold substrate to have no significant surface speciation or dissolution of material into the droplets. Similarly, the SAM with a simple alkyl thiol is also expected to give a hydrophobic substrate and no other chemical speciation/dissolution. However, significant differences are expected for the SAM with the ammonium salt, which may be considered as a strong electrolyte. On exposure to water one would expect the counter ion to be released/dissolved into the drop. Similarly, the carboxylic acid group will undergo some extent of deprotonation, although less than the ammonium salt as it is a weak acid. There are significant elements of complexity surrounding surface speciation and the amount of surface dissociation/charging. For example, once some species have been lost from a surface, giving a charged substrate, that charge prevents further ion release. This behaviour is well documented in works on solution speciation and environmental chemistry [53,54]. Hence the droplet formation behaviour in Fig. 8 is broadly in line with that expected for the capacity for surface speciation/dissolution.

In the Supplementary data we present order of magnitude calculations for the magnitude of the chemical potential/osmotic pressure for a strong electrolyte (e.g. the quaternary ammonium salt) and a weak acid (e.g. carboxylic acid and SiOH surface groups). These are found to be of the appropriate order required for the driving force for droplet formation.

The calculations also indicate that a small drop will have a relatively large driving potential which reduces as the droplets grow. Hence we expect the droplets initially to grow quickly but then slow down and essentially stop, as observed (Fig. 5).

The behaviour of the alcohol SAM is more interesting. One would expect the dissociation of the terminal-OH to be very small indeed, effectively negligible. Hence one would expect a surface with water loving OH groups which might be expected to give a wetting layer and not droplets at all. However, initially there do appear to be droplets (with a contact angle of approximately  $26^\circ$ ). This is attributed to a combination of the hydrophilic OH groups and the hydrophobic  $\text{CH}_2$  groups of the alkyl chain. However, as demonstrated above, the interfacial energy is unfavourable for any non-zero contact angle. At this time we do not have a clear explanation for the OH thiol droplet behaviour.

The kinetics of growth and shrinkage of a water drop at the oil/hydrophobic interface has been experimentally investigated and successfully compared to a mass transport model. Good agreement for a wide variety of oils with very different viscosities have been captured. The variation with chemical potential driving force has also shown to be an effective description. Significantly we have demonstrated that a very small chemical potential difference drives droplet formation. This was established by counter balancing the growth chemical potential by adding salts to the water reservoir which leads to droplet shrinkage. Interestingly, the water mobility through the oil does not vary with the oil viscosity but is a weak function of the silicone oil molecular weight, in excellent agreement with the literature.

The ultimate driving force for the droplet formation, however, remains unclear. Several potential driving forces have been considered here including interfacial free energies, buoyancy, *etc.*, however, none are expected to give the behaviour observed. Here we have proposed that surface chemistry/speciation/dissociation may be responsible. Many surfaces that form droplets have the potential for surface site dissociation, *e.g.* SiOH can lose a proton to give  $\text{SiO}^-$  and  $\text{H}^+$  [54]. (There is some evidence that OTS may also hydrolyse from the surface revealing SiOH groups). This kind of behaviour may lead to a small concentration in the otherwise pure water droplet that provides the very small chemical potential needed to drive the effect. Elementary calculations indicate the correct order of magnitude for the droplet

concentrations/chemical potentials. However, we are presently unable to prove the droplets attain the required pH or concentration of other dissolved species.

We have provided circumstantial evidence for this mechanism with a series of SAMs on gold where the likely extent of surface dissociation is changing. The broad trends agree well with that expected from this surface dissociation model. This model would also be expected to give a final droplet size, rather than continual growth, in good agreement with observations.

## **5. Conclusions**

The formation of sessile drops on solid surfaces has a long history in surface science. Here we have focused on water droplets forming at the oil/solid interface, which has a number of important commercial applications, particularly enhanced oil recovery [55–58] and has been the subject of a series of interesting contributions addressing more fundamental aspects [4-6]. The somewhat ‘unexpected’ behaviour of hydrophilic water molecules spontaneously diffusing through a sparingly water-soluble oil to form droplets on hydrophobic substrates was first reported in 2010 [4]. Other studies have since been conducted on these water/oil/solid sandwich systems to investigate this unusual phenomenon and have identified this to be a widespread behaviour, with droplet formation observed for combinations of a variety of oils and different chemistries of the underlying substrate [4-6, 33, 45]. However, the underlying driving force has not been identified.

In comparison with previous studies, observing interfacial droplet formation [4-6, 33, 45, 59], this is the first to present and consider possible mechanisms for the formation of interfacial droplets and to provide quantitative agreement with experiment. We advance the understanding in this area by considering water droplet formation/growth and shrinkage. Our data support a physical model for the kinetics of the process and uniquely enable us to access the magnitude of the driving chemical potential. We also propose, and provide quantitative supporting evidence for, an underlying mechanism that can account for the observed behaviour, including changes with substrate, oils and water reservoir composition.



Growth and shrinkage of water droplets are kinetically controlled by the difference in chemical potential between the substrate and the aqueous reservoir. The kinetics are described quantitatively by a mass transport model, with the droplet radius changing as  $a^2 \propto t$ . The constant of proportionality in this relationship provides an estimate of the chemical potential driving growth/shrinkage of the droplets. Interestingly this is found to be rather small.

The new physiochemical model for the driving force of droplet formation is based on surface chemistry/speciation/dissolution. For the small water droplets formed, this release of species into the droplet gives a small, but sufficient, chemical potential to overcome the other unfavourable free energy terms (such as the surface free energy). Our calculations indicate that the extent of surface dissociation/dissolution are of the correct order of magnitude for this effect.

Significantly, this surface speciation is common to many, indeed most, solid substrates from inorganic oxides to the organic SAMs, mentioned here. Hence this subtle dissociation/dissolution behaviour is expected to be rather general [60] and hence may have a range of implications for other interfaces should make a contribution in fundamental scientific innovation within interfacial processes, capillarity and wetting. We expect this to be a significant factor particularly in very low ionic strength conditions. At higher ionic strength, the background electrolyte concentration may swamp the more subtle effects outlined here.

A number of studies have reported the spontaneous formation of nanobubbles at interfaces, which may be considered to be related to the formation of water droplets at oil-solid interfaces addressed here. Nanobubbles at water-solid interfaces [61-63] are also characterized by one phase spontaneously forming between two immiscible phases. However, the current mechanism of surface dissolution would not be expected to act in that case – ions cannot dissolve in a vapour. This indicates that an alternative driving force is involved.

Water droplet condensation on hydrophobic surfaces has also been reported with LIS systems. These surfaces have a supported liquid that acts as an exposed surface for a solid, exploited as low friction substrates and other applications e.g. dew harvesting and

desalination, which exploit the condensation behaviour. The water droplets which condense on this essentially hydrophobic surface, and can roll off under the force of gravity [64-67].

Further investigation is needed to elucidate and confirm the proposed mechanism and to direct the rational design for controlling and potentially exploiting such interfacial phenomena, such as surface emulsification, [68,69] anti-corrosion, [70,71] water collection, [72,73] and mass transportation across interfaces [25,74].

### **Acknowledgement**

This work was supported by National Natural Science Foundation of China (21872078).

### **Declaration of interests**

The authors declare that they have no known competing financial interests or personal relationships that could have appeared to influence the work reported in this paper.

### **References**

- [1] E. Donaldson, W. Alam, Wettability, Gulf Publishing Company, 2008.
- [2] F.M. Fowkes, Hydrophobic Surfaces, Academic Press, 1969.
- [3] H.-J. Butt, K. Graf, M. Kappl, Physics and Chemistry of Interfaces, Wiley-VCH Verlag GmbH & Co. KGaA: Weinheim, 2004.
- [4] Z. Yang, N.L. Abbott, Spontaneous Formation of Water Droplets at Oil-Solid Interfaces, *Langmuir* 26 (2010) 13797–13804.
- [5] Y. Wang, Y. Wang, M. Cai, H. Li, Z. Yang, Preparation and Growth of Interfacial Ultrasmall Water Droplets between Alkanes and Hydrophobic Solid, *Chem. J. Chinese Universities* 39 (2018) 2003–2009.
- [6] R. Zhang, W. Liao, Y. Sun, J.Y.Y. Heng, Z. Yang, Investigating the Role of Glass and Quartz Substrates on the Formation of Interfacial Droplets, *J. Phys. Chem. C* 123 (2019) 1151–1159.
- [7] D. Gurera, B. Bhushan, Optimization of Bioinspired Conical Surfaces for Water Collection From Fog, *J. Colloid Interface Sci.* 551 (2019) 26–38.
- [8] H. Kim, S. Yang, S.R. Rao, S. Narayanan, E.A. Kapustin, H. Furukawa, A.S. Umans, O.M. Yaghi, E.N. Wang, Water Harvesting from Air with Metal-Organic Frameworks Powered by Natural Sunlight, *Science* 434 (2017) 430–434.
- [9] A. Méndez-Vilas, A.B. Jódar-Reyes, M.L. González-Martín, Ultrasmall Liquid

- Droplets on Solid Surfaces: Production, Imaging, and Relevance for Current Wetting Research, *Small* 5 (2009) 1366–1390.
- [10] P. Kim, M.J. Kreder, J. Alvarenga, J. Aizenberg, Hierarchical or Not? Effect of the Length Scale and Hierarchy of the Surface Roughness on Omniphobicity of Lubricant-Infused Substrates, *Nano Lett.* 13 (2013) 1793–1799.
- [11] Q. Li, Z. Guo, Lubricant-Infused Slippery Surfaces: Facile Fabrication, Unique Liquid Repellence and Antireflective Properties, *J. Colloid Interface Sci.* 536 (2019) 507–515.
- [12] S. Anand, A.T. Paxson, R. Dhiman, J.D. Smith, K.K. Varanasi, Enhanced Condensation on Lubricant-Impregnated Nanotextured Surfaces, *ACS Nano* 6 (2012) 10122–10129.
- [13] J.D. Smith, R. Dhiman, S. Anand, E. Reza-Garduno, R.E. Cohen, G.H. McKinley, K.K. Varanasi, Droplet Mobility on Lubricant-Impregnated Surfaces, *Soft Matter* 9 (2013) 1772–1780.
- [14] K. Rykaczewski, S. Anand, S.B. Subramanyam, K.K. Varanasi, Mechanism of Frost Formation on Lubricant-Impregnated Surfaces, *Langmuir* 29 (2013) 5230–5238.
- [15] D.J. Preston, Y. Song, Z. Lu, D.S. Antao, E.N. Wang, Design of Lubricant Infused Surfaces, *ACS Appl. Mater. Interfaces* 9 (2017) 42383–42392.
- [16] S. Anand, K. Rykaczewski, S.B. Subramanyam, D. Beysens, K.K. Varanasi, How Droplets Nucleate and Grow on Liquids and Liquid Impregnated Surfaces, *Soft Matter* 11 (2015) 69–80.
- [17] X. Zhang, J. Wang, L. Bao, E. Dietrich, R.C.A. van der Veen, S. Peng, J. Friend, H.J.W. Zandvliet, L. Yeo, D. Lohse, Mixed Mode of Dissolving Immersed Nanodroplets at a Solid-Water Interface, *Soft Matter* 11 (2015) 1889–1900.
- [18] Q. Xie, J. Harting, The Effect of the Liquid Layer Thickness on the Dissolution of Immersed Surface Droplets, *Soft Matter* 15 (2019) 6461–6468.
- [19] T. Kajiyama, F. Schellenberger, P. Papadopoulos, D. Vollmer, H.-J. Butt, 3D Imaging of Water-Drop Condensation on Hydrophobic and Hydrophilic Lubricant-Impregnated Surfaces, *Sci. Rep.* 6 (2016) 23687.
- [20] D. Lohse, X. Zhang, Surface Nanobubbles and Nanodroplets, *Rev. Mod. Phys.* 87 (2015) 981–1035.
- [21] S. Karpitschka, A. Pandey, L.A. Lubbers, J.H. Weijs, L. Botto, S. Das, B. Andreotti, J.H. Snoeijer, Liquid Drops Attract or Repel by the Inverted Cheerios Effect, *Proc. Natl. Acad. Sci. USA* 113 (2016) 7403–7407.
- [22] A. Bahramian, A. Zorbakhsh, Interfacial Equation of State for Ionized Surfactants at Oil/Water Interfaces, *Soft Matter* 11 (2015) 6482–6491.
- [23] J. Meng, J.B. You, X. Zhang, Viscosity-Mediated Growth and Coalescence of Surface Nanodroplets, *J. Phys. Chem. C* 124 (2020) 12476–12484.
- [24] U. Frisch, S. Matarrese, R. Mohayaee, A Reconstruction of the Initial Conditions of the Universe by Optimal Mass Transportation, *Nature* 417 (2002) 6–8.
- [25] S.T. Rachev, L. Rüschemdorf, *Mass Transportation Problems, Volume I: Theory*, Springer Science & Business Media, 1998.
- [26] X. Yao, Y. Zhang, L. Du, J. Liu, J. Yao, Review of the Applications of

- Microreactors, *Renew. Sustain. Energy Rev.* 47 (2015) 519–539.
- [27] B. Ahmed-omer, C. Brandt, T. Wirth, Advanced Organic Synthesis Using Microreactor Technology, *Org. Biomol. Chem.* 5 (2007) 733–740.
- [28] Z. Chu, Y. Feng, S. Seeger, Oil/Water Separation with Selective Superantiwetting/Superwetting Surface Materials, *Angew. Chem. Int. Ed.* 54 (2015) 2328–2338.
- [29] F. Li, B. Bhushan, Y. Pan, X. Zhao, Bioinspired Superoleophobic/Superhydrophilic Functionalized Cotton for Efficient Separation of Immiscible Oil-Water Mixtures and Oil-Water Emulsions, *J. Colloid Interface Sci.* 548 (2019) 123–130.
- [30] J. Sabaté del Río, O.Y.F. Henry, P. Jolly, D.E. Ingber, An Antifouling Coating That Enables Affinity-Based Electrochemical Biosensing in Complex Biological Fluids, *Nat. Nanotech.* 14 (2019) 1143–1149.
- [31] D.M. Yebra, S. Kiil, K. Dam-Johansen, Antifouling Technology – Past, Present and Future Steps Towards Efficient and Environmentally Friendly Antifouling Coatings, *Prog. Org. Coatings* 50 (2004) 75–104.
- [32] T. Young, An Essay on the Cohesion of Fluids, *Philos. Trans. R. Soc.* 95 (1805) 65–87.
- [33] Y. Li, Q. Yang, R.A. Mei, M. Cai, J.Y.Y. Heng, Z. Yang, Controlling the Accumulation of Water at Oil–Solid Interfaces with Gradient Coating, *J. Phys. Chem. B* 121 (2017) 6766–6772.
- [34] J.T. Su, P.B. Duncan, A. Momaya, A. Jutila, D. Needham, The Effect of Hydrogen Bonding on the Diffusion of Water in n-Alkanes and n-Alcohols Measured with a Novel Single Microdroplet Method, *J. Chem. Phys.* 132 (2010) 044506.
- [35] C. Sutton, J.A. Calder, Solubility of Higher-Molecular-Weight n-Paraffins in Distilled Water and Sea Water, *Environ. Sci. Technol.* 8 (1974) 654–657.
- [36] N. Watanabe, Y. Yasuda, K. Kato, T. Nakamura, Determination of Trace Amounts of Siloxanes in Water, Sediments and Fish Tissues by Inductively Coupled Plasma Emission Spectrometry, *Sci. Total Environ.* 34 (1984) 169–176.
- [37] C.A. Boundaries, [www.gelest.com/wp-content/uploads/Goods-PDF-brochures-inert\\_silicones\\_2013.pdf](http://www.gelest.com/wp-content/uploads/Goods-PDF-brochures-inert_silicones_2013.pdf), Gelest, Inc. Tech. Broch. (2013).
- [38] D. Wu, V. Hornof, Dynamic Interfacial Tension in Hexadecane/Water Systems Containing Ready-Made and In-Situ-Formed Surfactants, *Chem. Eng. Commun.* 172 (2007) 85–106.
- [39] H. Miyazaki, S. Inasawa, Drying Kinetics of Water Droplets Stabilized by Surfactant Molecules or Solid Particles in a Thin Non-Volatile Oil Layer, *Soft Matter* 13 (2017) 8990–8998.
- [40] M. Harz, M. Knoche, Droplet Sizing Using Silicone Oils, *Crop Prot.* 20 (2001) 489–498.
- [41] N. Watanabe, T. Nakamura, E. Watanabe, Bioconcentration Potential of Polydimethylsiloxane (PDMS) Fluids By Fish, *Sci. Total Environ.* 38 (1984) 167–172.
- [42] S.A. Mirji, Octadecyltrichlorosilane Adsorption Kinetics on Si(100)/SiO<sub>2</sub>

- Surface: Contact Angle, AFM, FTIR and XPS Analysis, *Surf. Interface Anal.* 38 (2006) 158–165.
- [43] F. Barca, T. Caporossi, S. Rizzo, Silicone Oil: Different Physical Properties and Clinical Applications, *Biomed Res. Int.* 2014 (2014) 502143.
- [44] T. Svitova, O. Theodoly, S. Christiano, R.M. Hill, C.J. Radke, Wetting Behavior of Silicone Oils on Solid Substrates Immersed in Aqueous Electrolyte Solutions, *Langmuir* 18 (2002) 6821–6829.
- [45] R. Zhang, Y. Wang, Z. Yang, Spatially Arranging Interfacial Droplets at the Oil-Solid Interface, *Soft Matter* 16 (2020) 107–113.
- [46] Y. Liu, X. Zhang, Evaporation Dynamics of Nanodroplets and Their Anomalous Stability on Rough Substrates, *Phys. Rev. E* 88 (2013) 012104.
- [47] X. Chen, R. Ma, J. Li, C. Hao, W. Guo, B.L. Luk, S.C. Li, S. Yao, Z. Wang, Evaporation of Droplets on Superhydrophobic Surfaces: Surface Roughness and Small Droplet Size Effects, *Phys. Rev. Lett.* 109 (2012) 116101.
- [48] A.J.D. Shaikkea, S. Basu, A. Tyagi, S. Sharma, R. Hans, L. Bansal, Universal Representations of Evaporation Modes in Sessile Droplets, *PLoS One* 12 (2017) e0184997.
- [49] S. Dash, S. V. Garimella, Droplet Evaporation Dynamics on a Superhydrophobic Surface with Negligible Hysteresis, *Langmuir* 29 (2013) 10785–10795.
- [50] X. He, J. Cheng, C.P. Collier, B.R. Srijanto, D.P. Briggs, Evaporation of Squeezed Water Droplets between Two Parallel Hydrophobic/Superhydrophobic Surfaces, *J. Colloid Interface Sci.* 576 (2020) 127–138.
- [51] E.L. Cussler, *Diffusion: Mass Transfer in Fluid Systems*, Cambridge University Press, 1984.
- [52] A.E. Ismail, G.S. Grest, D.R. Heine, M.J. Stevens, Interfacial Structure and Dynamics of Siloxane Systems: PDMS-Vapor and PDMS-Water, *Macromolecules* 42 (2009) 3186–3194.
- [53] W. Stumm, J.J. Morgan, *Aquatic Chemistry: Chemical Equilibria and Rates in Natural Waters*, Wiley-Interscience, 1970.
- [54] R.K. Iler, *The Chemistry of Silica: Solubility, Polymerization, Colloid and Surface Properties and Biochemistry of Silica*, Wiley-Blackwell, 1979.
- [55] M.J. Blunt, Q. Lin, T. Akai, B. Bijeljic, A Thermodynamically Consistent Characterization of Wettability in Porous Media Using High-Resolution Imaging, *J. Colloid Interface Sci.* 552 (2019) 59–65.
- [56] H.S. Rabbani, V. Joekar-Niasar, N. Shokri, Effects of Intermediate Wettability on Entry Capillary Pressure in Angular Pores, *J. Colloid Interface Sci.* 473 (2016) 34–43.
- [57] Y. Liu, A. Hansen, E. Block, N.R. Morrow, J. Squier, J. Oakey, Two-Phase Displacements in Microchannels of Triangular Cross-section, *J. Colloid Interface Sci.* 507 (2017) 234–241.
- [58] K.M. Askvik, S. Høiland, P. Fotland, T. Barth, T. Grønn, F.H. Fadnes, Calculation of Wetting Angles in Crude Oil/Water/Quartz Systems, *J. Colloid Interface Sci.* 287 (2005) 657–663.

- [59] R. Zhang, R.A. Mei, L. Botto, Z. Yang, Modified Voronoi Analysis of Spontaneous Formation of Interfacial Droplets on Immersed Oil-Solid Substrates, *Langmuir* 36 (2020) 5400–5407.
- [60] W. Stumm, J.J. Morgan, *Aquatic Chemistry: Chemical Equilibria and Rates in Natural Waters*, John Wiley & Sons, Inc., 1995.
- [61] J.L. Parker, P.M. Claesson, P. Attard, Bubbles, Cavities, and the Long-Ranged Attraction between Hydrophobic Surfaces, *J. Phys. Chem.* 98 (1994) 8468–8480.
- [62] S. Lou, Z. Ouyang, Y. Zhang, X. Li, J. Hu, M. Li, F. Yang, Nanobubbles on Solid Surface Imaged by Atomic Force Microscopy, *J. Vac. Sci. Technol. B* 18 (2000) 2573–2575.
- [63] N. Ishida, T. Inoue, M. Miyahara, K. Higashitani, Nano Bubbles on a Hydrophobic Surface in Water Observed by Tapping-Mode Atomic Force Microscopy, *Langmuir* 16 (2000) 6377–6380.
- [64] K.A. Wier, T.J. McCarthy, Condensation on Ultrahydrophobic Surfaces and Its Effect on Droplet Mobility: Ultrahydrophobic Surfaces are not Always Water Repellant, *Langmuir* 22 (2006) 2433–2436.
- [65] C. Dorrer, J. R uhe, Condensation and Wetting Transitions on Microstructured Ultrahydrophobic Surfaces, *Langmuir* 23 (2007) 3820–3824.
- [66] J.B. Boreyko, C.-H. Chen, Self-Propelled Dropwise Condensate on Superhydrophobic Surfaces, *Phys. Rev. Lett.* 103 (2009) 184501.
- [67] N. Miljkovic, R. Enright, Y. Nam, K. Lopez, N. Dou, J. Sack, E.N. Wang, Jumping-Droplet-Enhanced Condensation on Scalable Superhydrophobic Nanostructured Surfaces, *Nano Lett.* 13 (2013) 179–187.
- [68] I.F. Guha, S. Anand, K.K. Varanasi, Creating Nanoscale Emulsions Using Condensation, *Nat. Commun.* 8 (2017) 1371.
- [69] A. Saha, A. Nikova, P. Venkataraman, V.T. John, A. Bose, Oil Emulsification Using Surface-Tunable Carbon Black Particles, *ACS Appl. Mater. Interfaces* 5 (2013) 3094–3100.
- [70] C. Cui, A.T.O. Lim, J. Huang, A Cautionary Note on Graphene Anti-Corrosion Coatings, *Nat. Nanotechnol.* 12 (2017) 834–835.
- [71] M.F. Montemor, Functional and Smart Coatings for Corrosion Protection: A Review of Recent Advances, *Surf. Coat. Technol.* 258 (2014) 17–37.
- [72] Y. Zheng, H. Bai, Z. Huang, X. Tian, F. Nie, Y. Zhao, J. Zhai, L. Jiang, Directional Water Collection on Wetted Spider Silk, *Nature* 463 (2010) 640–643.
- [73] H. Bai, L. Wang, J. Ju, R. Sun, Y. Zheng, L. Jiang, Efficient Water Collection on Integrative Bioinspired Surfaces with Star-Shaped Wettability Patterns, *Adv. Mater.* 26 (2014) 5025–5030.
- [74] M.Y. Koroleva, E.V. Yurtov, Water Mass Transfer in W/O Emulsions, *J. Colloid Interface Sci.* 297 (2006) 778–784.

# Supplementary Materials

## 1. Supplementary data

### 1.1. Droplet growth model

Consider a droplet in the form of a truncated sphere of radius  $a$  with contact angle  $\theta$  as shown in Fig. A1. The contact angle is assumed to remain constant, which was found in experiments to hold until the final stage of shrinkage. In the final stage the length of the contact line was found to remain constant, and the contact angle decreased. The transition between the constant contact angle and constant contact radius regimes (albeit the other way round) was discussed by Chen *et al.* (2011) [1].

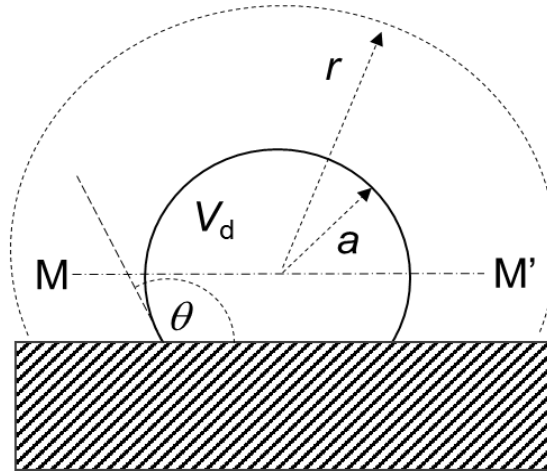


**Fig. A1.** Schematic illustrating the parameters characterizing the size of the droplets of interest.

When  $\theta > 90^\circ$ , it is likely that depletion (or saturation) of dissolved component in the region below the droplet midplane (M-M' in Fig. A1) would occur, so that in practice only the upper hemispherical surface would be active in terms of transport, with area  $A_{ow}$ .

$$A_{ow} = 2\pi a^2 \quad \dots[A1]$$

If the molar flux of water away from the surface of the drop is  $N_{w,a}$ , the growth of the drop follows

$$\frac{d}{dt} \left\{ \frac{1}{\bar{v}_w} \frac{\pi a^3}{3} \psi \right\} = -2\pi a^2 N_{w,a} \quad \dots[A2]$$

Hence

$$\frac{da}{dt} = -\frac{2}{\psi} \bar{v}_w N_{w,a} \quad \dots[A3]$$

It should be noted that the above model assumes that  $N_{w,a}$  is uniform over the droplet

surface. This could be quantified by numerical simulation but is not attempted here as the general form of this first order model is not changed.

Let the mol fraction of water in the aqueous phase be  $x$  and the mol fraction of water in the oil phase be  $y$ . The latter is expected to be small so Henry's law is assumed to apply, with equilibrium constant  $K$ .

$$y = Kx \quad \dots[A4]$$

Growth is slow: assuming instantaneous steady state allows diffusion in the oil phase to be described, in spherical co-ordinates, as

$$N_w = -\frac{D}{\bar{V}_o(1-y)} \frac{dy}{dr} \quad \dots[A5]$$

where  $N_w$  is the flux at location  $r$  ( $r \geq a$ ),  $\bar{V}_o$  is the molar volume of the oil and  $D$  is a Fickian diffusion coefficient. For the dilute case,  $-d \ln(1-y) dr \approx dy/dr$ . Assuming spherical symmetry, conservation of mass allows one to write [A5] in terms of the flux at the droplet surface

$$N_w = N_{w,a} \frac{a^2}{r^2} = -\frac{D}{\bar{V}_o} \frac{dy}{dr} \quad \dots[A6]$$

Integrating from  $r = a$  to great distance (the film is relatively thick so we approximate the upper limit to be infinity) yields

$$N_{w,a} = \frac{D}{\bar{V}_o} \frac{1}{a} (y(a) - y(\infty)) = \frac{KD}{\bar{V}_o} \frac{1}{a} (x(a) - x(\infty)) \quad \dots[A7]$$

Hence if the droplet contains pure water and the liquid phase is saline, the RHS is positive and water diffuses away from the droplet. Conversely, if the droplet grows when the top reservoir is pure water, Equation [A7] indicates that  $x(a) < 1$ , *i.e.* the droplet does not contain pure water. A more detailed interpretation, however, would require the transport equations to be written in terms of difference in chemical potential (see Cussler [2]).

The above caveats notwithstanding, the droplet growth law can be written as

$$\frac{da}{dt} = -\frac{2}{\psi} KD \frac{\bar{V}_w}{\bar{V}_o} \frac{1}{a} \Delta x = -\frac{k_1}{a} \Delta x \quad \dots[A8]$$

Here  $k_1$  is a group of physical and geometrical parameters and is the difference in water mol fractions between the droplet and the aqueous reservoir. Integrating from radius  $a_0$



at time zero gives

$$a^2 = a_0^2 - (2k_1\Delta x)t = a_0^2 - Bt \quad \dots[\text{A9}]$$

Or, in terms of droplet volume,

$$B \propto K \frac{\bar{V}_w^{1.4}}{M/\rho} \frac{M^{1/2}}{\mu} \Delta\Pi = K \frac{\bar{V}_w^{1.4}}{\nu M^{1/2}} \Delta\Pi \quad \dots[\text{A10}]$$

It is convenient to work in terms of osmotic pressure,  $\Pi$ . For sufficiently dilute solutions, where the mol fraction of solute is  $1-x$ , the Van't Hoff equation, gives

$$\frac{da}{dt} = \frac{2KD}{\psi} \frac{\bar{V}_w}{a} \frac{\bar{V}_w \Delta\Pi}{RT} = \frac{k_2}{a} \Delta\Pi \quad \dots[\text{A11}]$$

where  $\Delta\Pi$  is the difference in osmotic pressures between the reservoir and the droplet phases. A plot of  $a^2$  against time should be linear with gradient,  $B$ , proportional to  $\Delta\Pi$ .

Cussler reports the form of the Wilke-Chang result for estimating the diffusivity of water in an oil as

$$D = \frac{7.4 \times 10^{-15} (2.6M)^{1/2} T}{\mu \bar{V}_w^{0.6}} \quad \dots[\text{A12}]$$

where the molecular mass of the oil is in Daltons and  $\bar{V}_w$  is in  $\text{cm}^3\text{mol}^{-1}$ . Substituting this result into [A11] gives the expected dependency of  $B$  on liquid properties as

$$B \propto K \frac{\bar{V}_w^{1.4}}{\bar{V}_o} \frac{M^{1/2}}{\mu} \Delta\Pi \quad \dots[\text{A13}]$$

The molar volume of the oil can be estimated from its density,  $\rho$ , giving

$$B \propto K \frac{\bar{V}_w^{1.4}}{M/\rho} \frac{M^{1/2}}{\mu} \Delta\Pi = K \frac{\bar{V}_w^{1.4}}{\nu M^{1/2}} \Delta\Pi \quad \dots[\text{A13}]$$

where  $\nu$  is the dynamic viscosity of the oil. Fig. A2 shows the dependency of  $\nu$  on  $M$  for a series commercial silicon oils, as  $\nu \sim M^{1.5}$ . Substituting this into Eqn. [A13] yields  $B \propto M^{-2} \Delta\Pi$

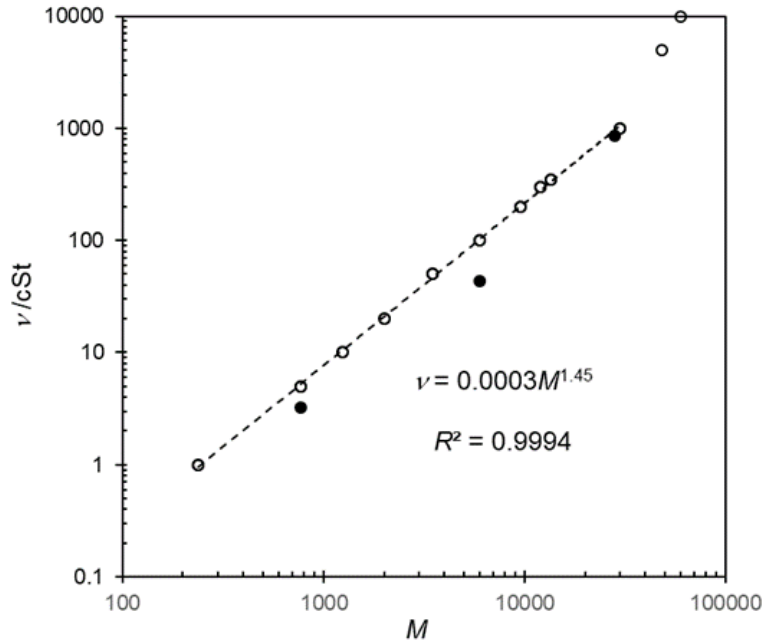


**Fig. A2.** Effect of molecular mass  $M$  on dynamic viscosity of PDMS oils. Open symbols – Mojsiewicz-Pieńkowska, K. (2012) [3]; solid symbols – oils used in this work. Dashed line shows power law fit to Mojsiewicz-Pieńkowska data for range  $1 < \nu < 1000$  cSt.

## 1.2. Surface Dissociation Calculation

The following calculations provide estimates of the associated change in chemical potential and osmotic pressure on surface dissociation/dissolution. As noted above some substrates have a surface layer with a strong electrolyte, expected to fully dissociate in water (quaternary ammonium salt) and a weak acid substrate (e.g. carboxylic acid and SiOH groups), that are expected to only partially dissociate.

For illustrative purposes we consider the SiOH case assuming it is a) a strong, fully dissociated electrolyte and b) only partially dissociated. The strongest chemical potential will be the strong electrolyte case.

### A) ‘Strong electrolyte case’

Consider a droplet of radius  $a$  and contact angle  $\theta$ . The wetted area in contact with the layer per unit drop volume is  $\pi a^2 \sin^2 \theta$ . There are a range of values reported for the number density of Si-OH on silica [4] from  $21.7 \text{ \AA}^2$  per SiOH site, although free,

non-internally hydrogen bonded SiOH is  $71.4 \text{ \AA}^2$  per SiOH site. Hence here we have approximated the SiOH site density as  $50 \text{ \AA}^2$  per site. If each OH group was deprotonated completely (strong electrolyte case) this would give a surface site density,  $S_T$ , of  $3.3 \times 10^{-6} \text{ mol SiO}^- \text{ groups m}^{-2}$ . If this number of  $H^+$  ions was dispersed through the droplet volume the concentration would be. For a hemispherical drop ( $\theta = 90^\circ$ ) the concentration of  $H^+$  ions in solution would be  $5/a \text{ mol m}^{-3}$  (or  $5/a \text{ mmol dm}^{-3}$ ) where  $a$  is in  $\mu\text{m}$ . The associated osmotic pressure, estimated from the van't Hoff law, would be

$$\Pi = 9.9 \times 10^{-6} \frac{RT}{a} \frac{(1 + \cos\theta)}{(2 - \cos^2\theta)} \quad [\text{A14}]$$

Fig. A3 shows the effect of contact angle for a droplet with a set volume, expressed as the radius of a spherical droplet.

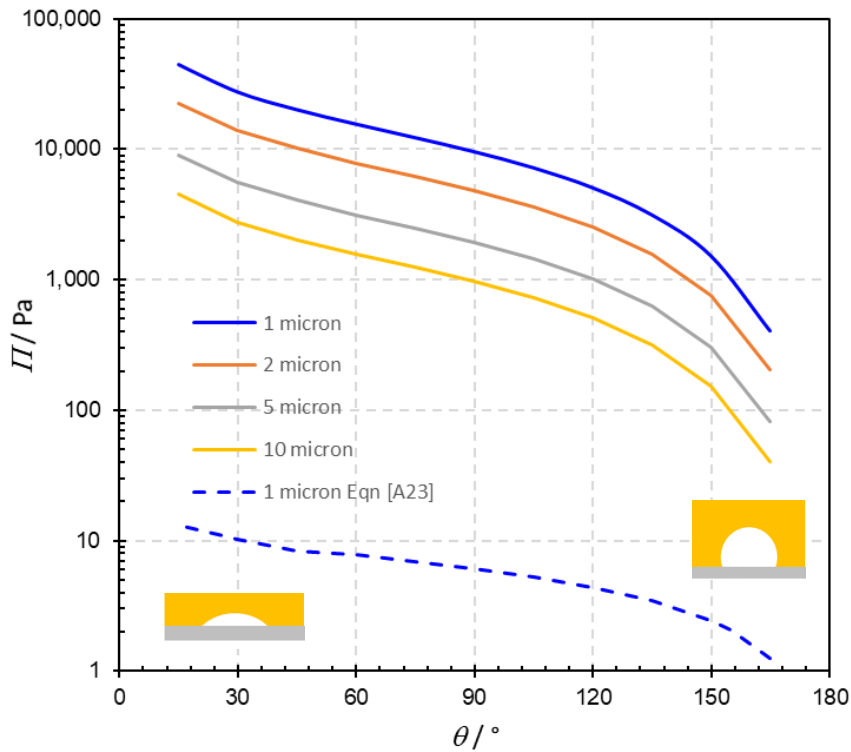


**Fig. A3** Effect of contact angle on estimated osmotic pressure. Solid loci show strong electrolyte relationship (Equation [A14]) for droplets of fixed volume, expressed as the radius of a sphere of that volume. As the contact angle increases, the droplet becomes more spherical and the wetted area per unit volume decreases. The dashed line shows the weak electrolyte result with equilibrium considered across the droplet (Equation [A23]) for a droplet with volume that of a  $1 \mu\text{m}$  sphere.

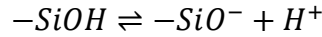
With a small contact angle the droplet takes the form of a lens with a relatively large wetted area, small drop volume and hence a relatively high  $H^+$  concentration and osmotic pressure. A larger contact angle changes the droplet shape to a truncated sphere, with a larger drop volume with a lower osmotic pressure. The osmotic pressure decreases with droplet volume.

*B) 'Weak electrolyte case'*

The simple model above does not account for partial dissolution of weak acids (carboxylic acid and SiOH). This calculation also requires electroneutrality in the drop and the autodissociation of water to be followed.

A detailed model of the distribution of charged species over the droplet is a challenging task, particularly in the absence of other dissolved species (background electrolyte). Local equilibrium at the SiOH surface is therefore considered to give an indication of the conditions there.

Assume that Si-OH groups dissociate as



with dissociation constant  $K_a^{SiOH}$ , such that

$$K_a^{SiOH} = \frac{[-SiO^-][H^+]_s}{[-SiOH]} \quad [A15]$$

where  $[-SiO^-]$  and  $[-SiOH]$  are surface concentrations and  $[H^+]_s$  is the concentration of  $H^+$  ions in solution at the wetted surface, in  $\text{mol dm}^{-3}$ .

This quantity is related to the concentration in the bulk,  $[H^+]$ , by

$$[H^+]_s = [H^+]e^{-\frac{ze\varphi_0}{k_B T}} \quad [A16]$$

where  $e$  is the elementary charge,  $z$  is charge number,  $k_B$  is the Boltzmann constant and  $\varphi_0$  the surface potential which arises from the surface dissociation. The surface charge is negative in this case, which attracts proton back to the surface, impeding further dissociation. Hence, we expect less dissolved species in the weak electrolyte case.

In this calculation we ignore the role of the surface potential and only include the weak acidity of the surface groups. Hence we assume that  $[H^+]_s \approx [H^+]$ . The total number of SiOH groups available (protonated and deprotonated) will be constant which is set by the number density,  $S_T$ , with  $S_T = [-SiOH] + [-SiO^-]$  and the area of the water droplet on the surface. Substituting this into [A15] gives

$$S_T = [-SiOH] + K_a^{SiOH} \frac{[-SiOH]}{[H^+]_s} = [-SiOH] \left\{ 1 + \frac{K_a^{SiOH}}{[H^+]_s} \right\} \quad [A17]$$

This yields

$$[-SiOH] = \frac{S_T}{\left\{ 1 + \frac{K_a^{SiOH}}{[H^+]_s} \right\}} \quad [A18]$$

and

$$[-SiO^-] = \frac{[H^+]_s S_T}{\{K_a^{SiOH} + [H^+]_s\}} \quad [A19]$$

Electroneutrality requires

$$n_{H^+} = n_{SiO^-} + n_{OH^-} \quad [A20]$$

Let us assume that the concentrations of  $H^+$  and  $OH^-$  are uniform throughout the droplet,  $[H^+]$  and  $[OH^-]$ , respectively. Equation [A20] can then be written as

$$[H^+] = \frac{A}{V} [-SiO^-] + [OH^-] \quad [A21]$$

where  $A/V$  is the wetted area per unit volume of the droplet, calculated above.

Combining [A19] and [A21] gives

$$[H^+] = \frac{A}{V} \frac{[H^+] S_T}{\{K_a^{SiOH} + [H^+]\}} + \frac{K_w}{[H^+]} \quad [A22]$$

which yields a cubic in  $[H^+]$ :

$$\begin{aligned} [H^+]^3 + [H^+]^2 K_a^{SiOH} + [H^+] \left\{ -K_a^{SiOH} \frac{A}{V} S_T - K_w \right\} - K_w K_a^{SiOH} \\ = 0 \end{aligned} \quad [A23]$$

Values of  $pK_a^{SiOH}$  in the literature lie in the range  $5.8 \pm 1.0$  [5]. With  $K_w = 10^{-14}$ ,

Equation [A23] can be solved for  $[H^+]$  where  $S_{TA}/V$  is in  $\text{mol dm}^{-3}$  from above.

Putting in the values of the parameters, the term  $K_w K_a^{SiOH}$  is very small and [A23] collapses to a quadratic. Fig. A3 shows the calculation for the 1  $\mu\text{m}$  volume droplet: the osmotic pressure is very much smaller than the strong electrolyte case, as expected.

In summary, we conclude that surface dissociation of a strong electrolyte provides a small, but significant chemical potential that could drive droplet formation. Weak electrolytes are expected to have a similar driving force but with a much smaller driving force, the magnitude of which will depend on the dissociation constant of the surface group.

We note that when a droplet initially forms, there are a relatively large number of surface sites for a small droplet volume, giving a high droplet concentration and large driving force leading to relatively rapid droplet growth. As the droplet grows the droplet concentration falls and the driving force for growth diminishes and the rate of growth will fall, until there is a very slow growth and the droplet appears to be essentially constant size.

## References

- [1] X. Chen, R. Ma, J. Li, C. Hao, W. Guo, B.L. Luk, S.C. Li, S. Yao, Z. Wang, Evaporation of Droplets on Superhydrophobic Surfaces: Surface Roughness and Small Droplet Size Effects, *Phys. Rev. Lett.* 109 (2012) 116101.
- [2] E.L. Cussler, *Diffusion: Mass Transfer in Fluid Systems*, Cambridge University Press, 1984.
- [3] K. Mojsiewicz-Pieńkowska, Size Exclusion Chromatography with Evaporative Light Scattering Detection as a Method for Speciation Analysis of Polydimethylsiloxanes. III. Identification and Determination of Dimeticone and Simecicone in Pharmaceutical Formulations, *J. Pharm. Biomed. Anal.* 58 (2012) 200–207.
- [4] R.K. Iler, *The Chemistry of Silica: Solubility, Polymerization, Colloid and Surface Properties and Biochemistry of Silica*, Wiley-Blackwell, 1979.
- [5] M. Sulpizi, M.P. Gaigeot, M. Sprik, The Silica-Water Interface: How the Silanols Determine the Surface Acidity and Modulate the Water Properties, *J. Chem. Theory Comput.* 8 (2012) 1037–1047.

## 2. Supplementary figures and tables

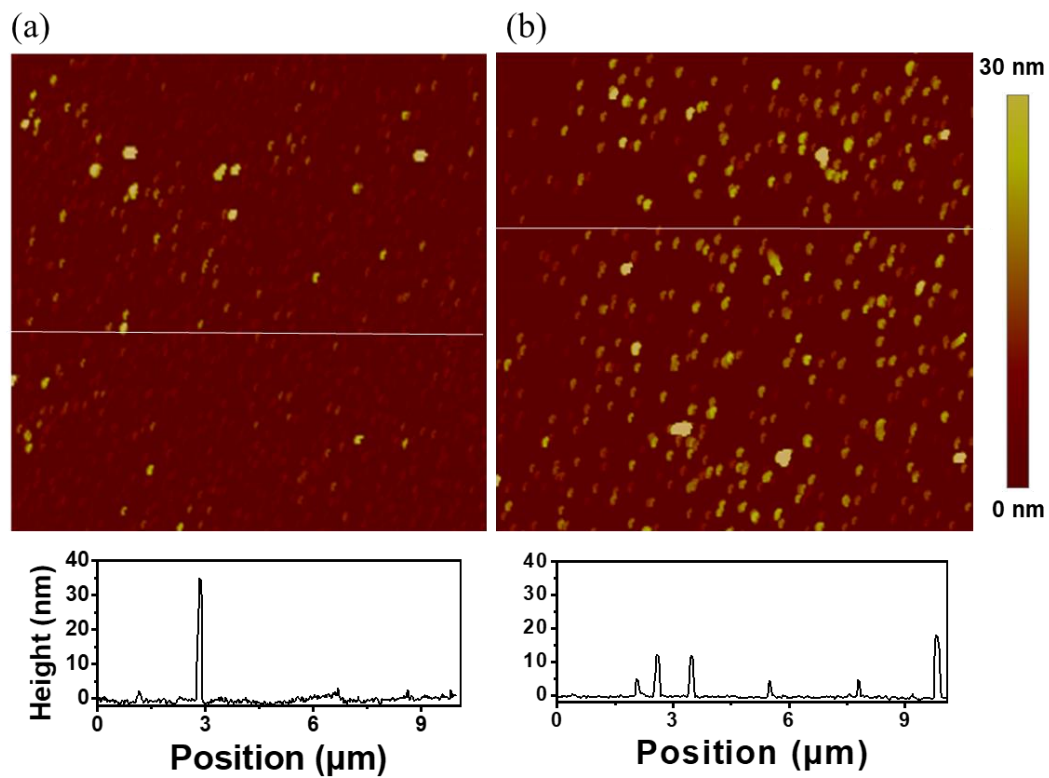


**Fig. S1.** AFM topography images of glass in air (tapping mode, scan size:  $10 \times 10 \mu\text{m}^2$ ) (a) before and (b) after piranha cleaning. The RMS roughness is (a) 2.22 nm and (b) 3.55 nm in an area of  $10 \times 10 \mu\text{m}^2$ .

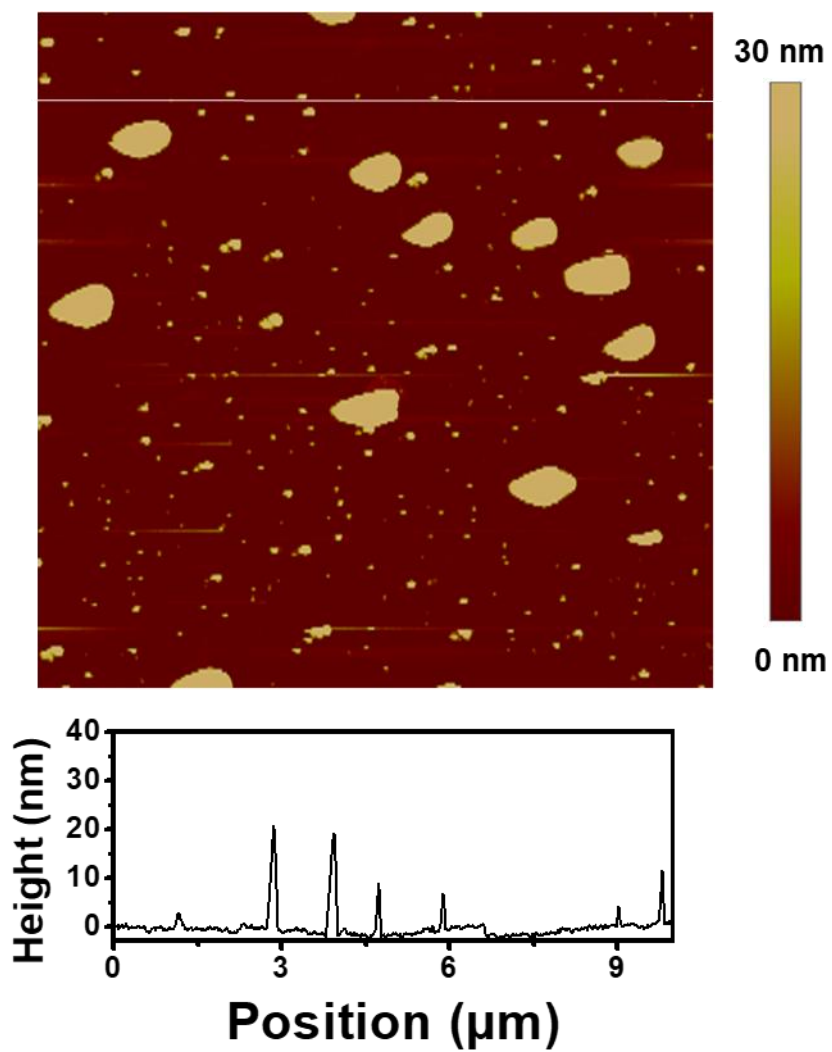


**Fig. S2.** AFM topography image of OTS-glass in air (tapping mode, scan size:  $10 \times 10 \mu\text{m}^2$ ). The RMS roughness of the substrate is 8.30 nm over an area of  $10 \times 10 \mu\text{m}^2$ .



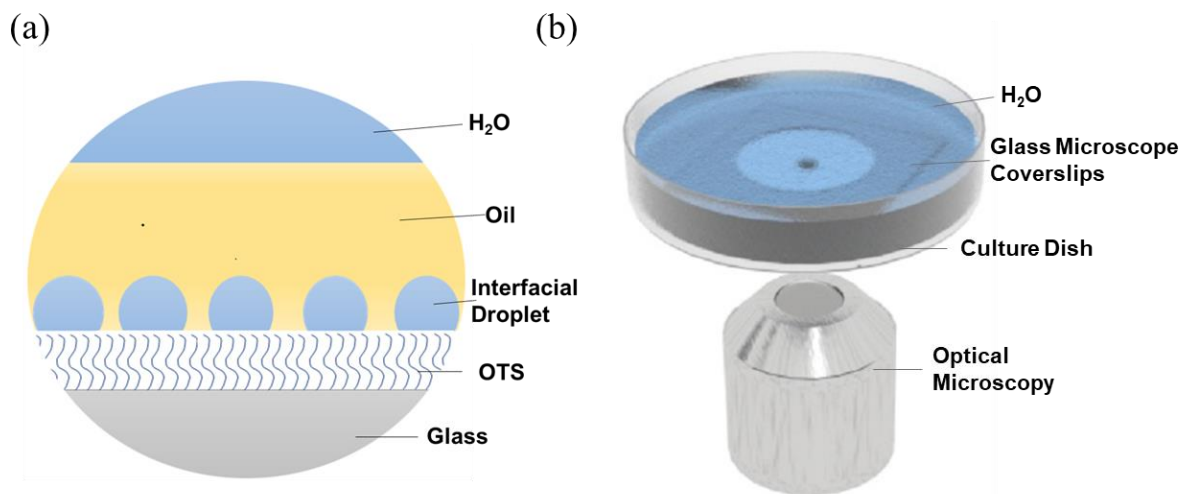


**Fig. S3.** Schematic illustrations of (a) the water/oil/solid sandwich structure, and (b) the experimental configuration allowing imaging of interfacial droplets at the centre of a petri dish located above the condensing lens of an optical microscope.

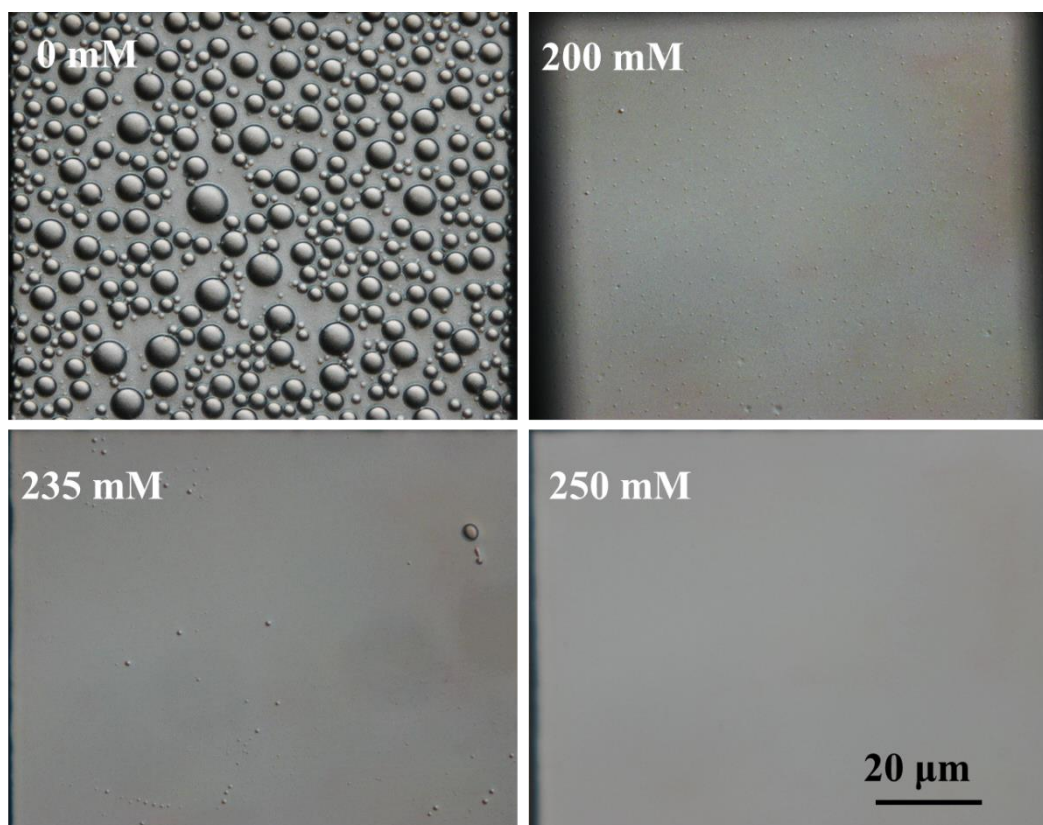


**Fig. S4.** Optical images of interfacial droplets at silicone oil 6000/OTS interfaces incubated for 7 days under different NaCl concentrations in the aqueous reservoir.

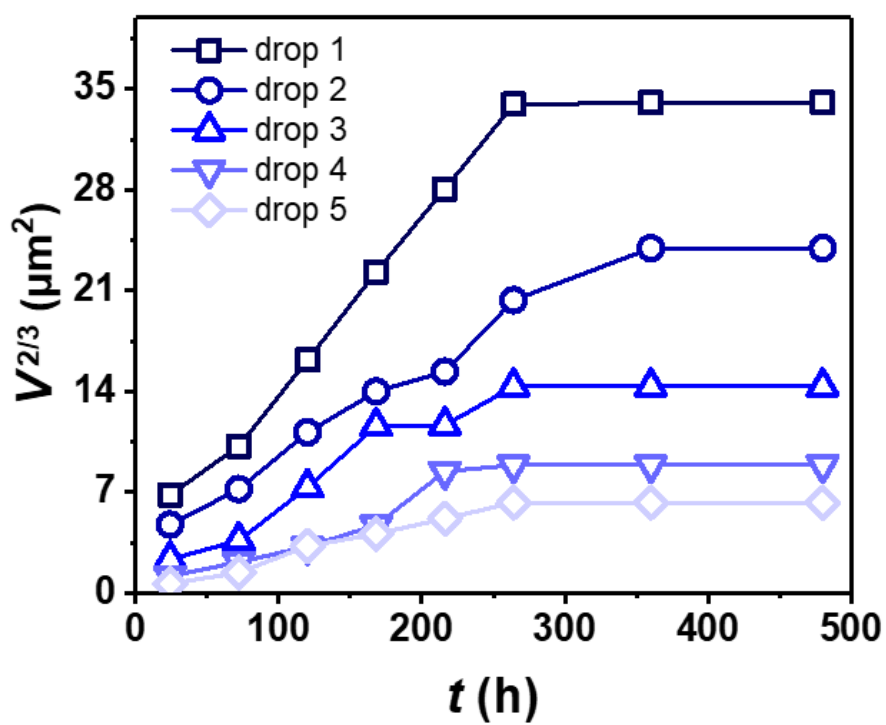
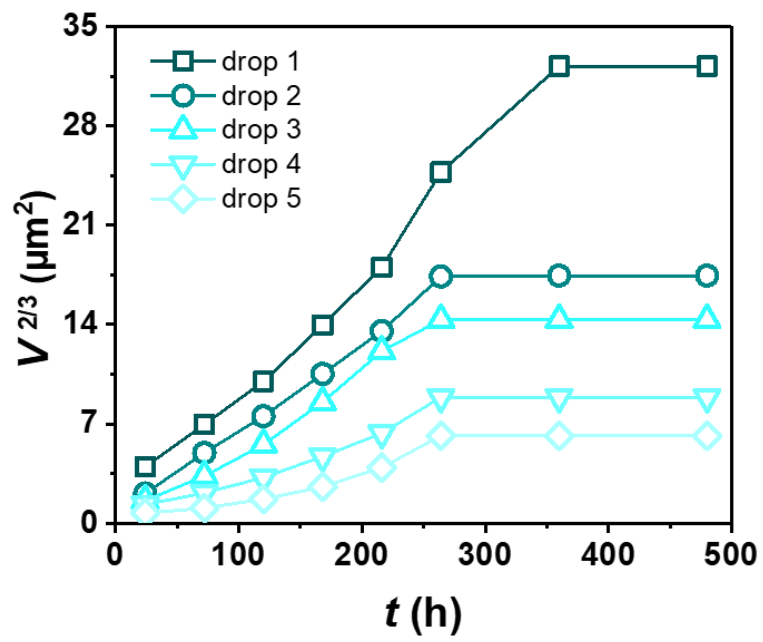
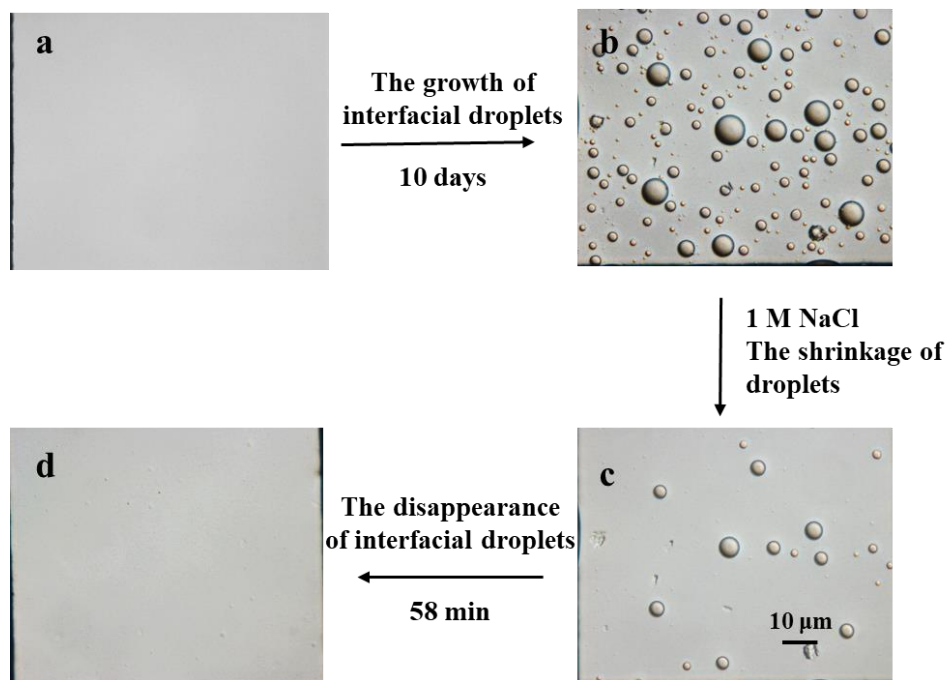


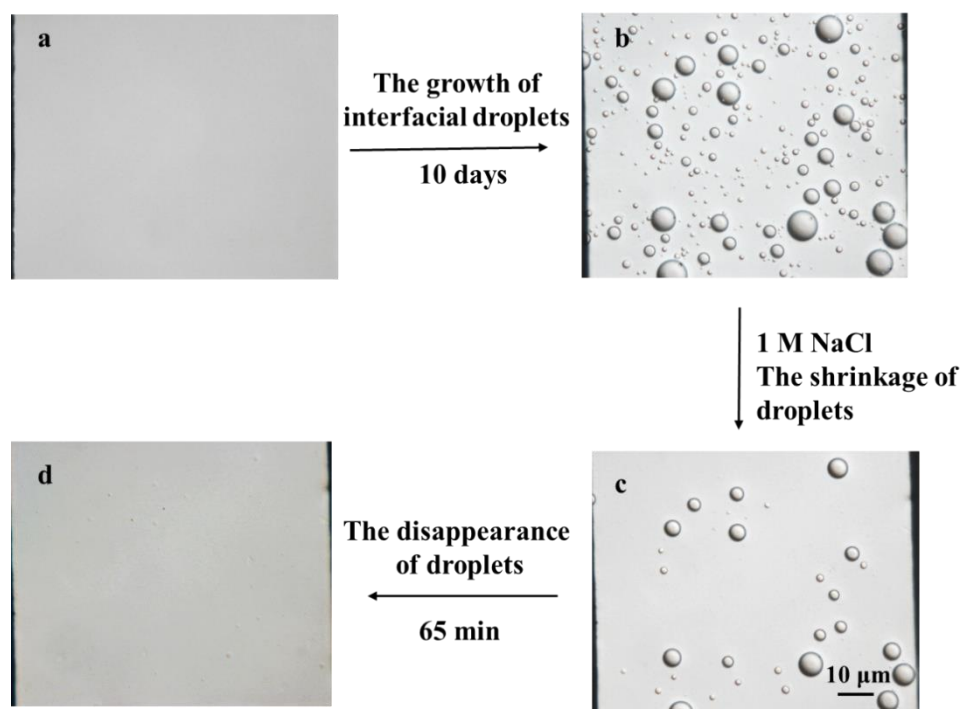
Fig. S5. Examples of droplet growth, time post nucleation, in silicone oil 770.



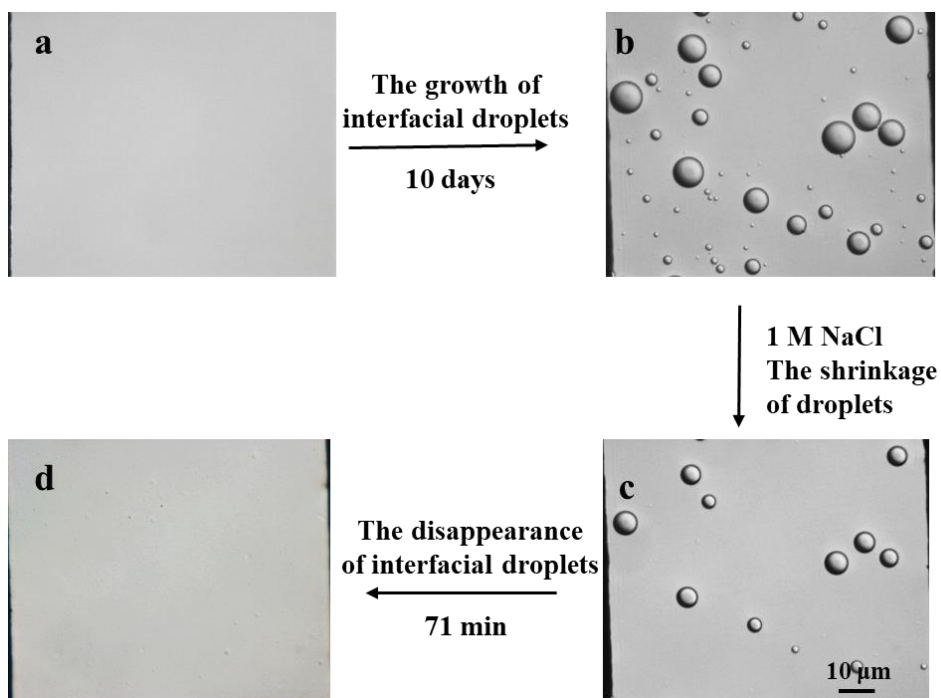
**Fig. S6.** Examples of droplet growth, time post nucleation, in silicone oil 28000.



**Fig. S7.** Representative microscope images of the growth and disappearance of interfacial droplets at the oil/solid interface for a silicone oil with molecular weight of 770. The growth of interfacial droplets between (a) day 0 and (b) day 10 is followed by rapid shrinking when the water reservoir is changed to 1 M NaCl solution, after (c) 20 min and (d) 58 min.

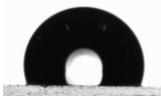





**Fig. S8.** Representative microscope images of the growth and disappearance of interfacial droplets at the oil/solid interface for a silicone oil with molecular weight of 6000. The growth of interfacial droplets between (a) day 0 and (b) day 10 is followed by rapid shrinking when the water reservoir is changed to 1 M NaCl solution, after (c) 20 min and (d) 65 min.



**Fig. S9.** Representative microscope images of the growth and disappearance of interfacial droplets at the oil/solid interface for a silicone oil with molecular weight of 28000. The growth of interfacial droplets between (a) day 0 and (b) day 10 is followed by rapid shrinking when the water reservoir is changed to 1 M NaCl solution, after (c) 20 min and (d) 71 min.

**Table S1** Contact angles of water and silicone oil ( $M=770, 6000, 28000$ ) on OTS-glass in air.

<b>Liquid</b>	<b>water</b>	<b>silicone oil 770</b>	<b>silicone oil 6000</b>	<b>silicone oil 28000</b>
<b>Contact angle</b>	$110.0^\circ \pm 0.2^\circ$	$11.2^\circ \pm 0.2^\circ$	$14.0^\circ \pm 0.6^\circ$	$15.3^\circ \pm 0.7^\circ$
				



**Table S2** Thickness of oil layer in tests with different silicone oils and reservoir NaCl loading, reported in Fig. 6. Each thickness value was the average of at least three measurements.

<b>Concentration</b>	<b>silicone oil 770</b>	<b>silicone oil 6000</b>	<b>silicone oil 28000</b>
<b>0.50 M</b>	56±0 μm	30±1 μm	37±4 μm
<b>0.75 M</b>	43±2 μm	40±1 μm	18±3 μm
<b>1.00 M</b>	79±4 μm	30±2 μm	22±0 μm
<b>1.50 M</b>	53±2 μm	28±2 μm	23±1 μm
<b>2.00 M</b>	47±2 μm	41±2 μm	22±3 μm

### 3. Supplementary code

The purpose of this Matlab code is to identify each droplet in the optical micrographs and extract its diameter automatically.

```
file_path = 'E:\ the disappearing drops\MATLAB\'; img_path_list =
dir(strcat(file_path, '*.jpg'));
img_num = length(img_path_list);
Num_title = zeros(size(img_path_list,1),1);
for q = 1:size(img_path_list, 1)
    Num_title(q, 1) = sscanf(img_path_list(q).name, '%d"*.jpg'); end
    [min_Num, oposition_Num] = min(Num_title);
image_name = img_path_list(oposition_Num).name; image = imread(strcat(file_path,
image_name));
image1 = rgb2gray(image); image1 = im2bw(image1);
image1 = ~image1(:,:,1); %figure, imshow(image1);
%PixelSensitivity = 10;
%image1 = bwareaopen(image1, PixelSensitivity);
[Original_centre, Original_radius] = imfindcircles(image1, [10 100]);
Num_columns = length(Original_centre);
A = 1:Num_columns;
A = A';
RGB = insertText(image, Original_centre, A); imwrite(RGB, ['E:\ the disappearing
drops\MATLAB\', 'datas.jpg']);
Statis_diameter = 1:Num_columns;
if img_num > 0
    for j = 1:img_num
        image_name = img_path_list(j).name;
        image = imread(strcat(file_path, image_name));
        %subplot(2, img_num, j), imshow(image);
        image1 = rgb2gray(image);
        image1 = im2bw(image1);
        image1 = ~image1(:,:,1);
        %figure, imshow(image1);
        %PixelSensitivity = 10;
        %image1 = bwareaopen(image1, PixelSensitivity);
        [centre, radius] = imfindcircles(image1, [20 100]);
        Num_new_columns = size(centre, 1);
        if ~isempty(centre)
            RGB = insertShape(image, 'Circle',[centre radius]);
            RGB = insertText(RGB, centre, radius);
            for m = 1:Num_new_columns
                for n = 1:Num_columns
                    if centre(m,1) < (Original_centre(n,1) +
```

```

Original_radius(n,1)) && centre(m,1) > (Original_centre(n,1) - Original_radius(n,1))
&& centre(m,2) < (Original_centre(n,2) + Original_radius(n,1)) && centre(m,2) >
(Original_centre(n,2) - Original_radius(n,1))
        Statis_diameter(j + 1, n) = radius(m);
        end
    end
end
    %subplot(2, img_num, j + img_num), imshow(RGB);
    imwrite(RGB, ['E:\ disappearing of drops \MATLAB\', image_name]);
else
    imwrite(image, ['E:\ disappearing of drops \MATLAB\',
image_name]);
    end
end
end
Num_title = [double(-1);Num_title];
collection_datas =[Num_title Statis_diameter];
collection_datas = sortrows(collection_datas, 1);
xlswrite('Collection_Datas', collection_datas);
clc, clear;

```